



HAL
open science

Hnf1b haploinsufficiency differentially affects developmental target genes in a new renal cysts and diabetes mouse model

Leticia L Niborski, Mélanie Paces-Fessy, Pierbruno Ricci, Adeline Bourgeois, Pedro Magalhães, Maria Kuzma-Kuzniarska, Celine Lesaulnier, Martin Rezko, Edwige Declercq, Petra Züribig, et al.

► To cite this version:

Leticia L Niborski, Mélanie Paces-Fessy, Pierbruno Ricci, Adeline Bourgeois, Pedro Magalhães, et al.. Hnf1b haploinsufficiency differentially affects developmental target genes in a new renal cysts and diabetes mouse model. *Disease Models & Mechanisms*, 2021, pp.dmm.047498. 10.1242/dmm.047498 . hal-03176214

HAL Id: hal-03176214

<https://hal.sorbonne-universite.fr/hal-03176214v1>

Submitted on 22 Mar 2021

HAL is a multi-disciplinary open access archive for the deposit and dissemination of scientific research documents, whether they are published or not. The documents may come from teaching and research institutions in France or abroad, or from public or private research centers.

L'archive ouverte pluridisciplinaire **HAL**, est destinée au dépôt et à la diffusion de documents scientifiques de niveau recherche, publiés ou non, émanant des établissements d'enseignement et de recherche français ou étrangers, des laboratoires publics ou privés.

Hnf1b haploinsufficiency differentially affects developmental target genes in a new Renal Cysts and Diabetes mouse model

Leticia L Niborski^{1#}, Mélanie Paces-Fessy^{1#}, Pierbruno Ricci^{1#}, Adeline Bourgeois¹, Pedro Magalhães^{2,3}, Maria Kuzma-Kuzniarska¹, Celine Lesaulnier¹, Martin Rezko⁴, Edwige Declercq¹, Petra Züribig², Alain Doucet⁵, Muriel Umbhauer¹ and Silvia Cereghini^{1*}

¹- Sorbonne Université, CNRS, Institut de Biologie Paris Seine, Laboratoire de Biologie du Développement, IBPS, UMR7622, F-75005 Paris, France

²- Mosaiques Diagnostics Hannover, Germany

³- Department of Pediatric Nephrology, Hannover Medical School, Hannover, Germany

⁴-BSRC AI. Fleming, Division of Molecular Biology & Genetics Genomics Facility- Athens Greece

⁵- Sorbonne Université, Université Paris Descartes, UMRS 1138; CNRS, ERL 8228, Centre de Recherche des Cordeliers, Paris, France.

These authors contributed equally to the work

* Silvia Cereghini corresponding author

Address: Institut de Biologie Paris-Seine (IBPS)

CNRS - UMR7622 Developmental Biology, bâtiment C, étage 7, case 24,

9 Quai Saint-Bernard, 75 252 PARIS CEDEX 05

Present address:

Leticia L Niborski: Centre de Recherche Institut Curie -75005 Paris - France

Pierbruno Ricci: Cepton Strategies 11 rue Lincoln, 75008, Paris- France

Key words: HNF1B, RCAD, gene dosage, Haploinsufficiency, glomerular and proximal tubules cysts, mouse model, transcriptomics

ABSTRACT

Heterozygous mutations in *HNF1B* cause the complex syndrome Renal Cysts and Diabetes (RCAD), characterized by developmental abnormalities of the kidneys, genital tracts and pancreas, and a variety of renal, pancreas and liver dysfunctions. The pathogenesis underlying this syndrome remains unclear as mice with heterozygous null mutations have no phenotype, while constitutive/conditional *Hnf1b*-ablation leads to more severe phenotypes.

We generated a novel mouse model carrying an identified human mutation at the intron-2 splice donor-site. Unlike heterozygous previously characterized, heterozygous for the splicing mutation exhibited decreased HNF1B protein levels and bilateral renal cysts from embryonic stage E15, originated from glomeruli, early proximal tubules (PT) and intermediate nephron segments, concurrently with a delayed PT differentiation, hydronephrosis and rare genital tract anomalies.

Consistently, mRNA-sequencing showed that most down-regulated genes in embryonic kidneys were primarily expressed in early PTs and Henle's Loop and involved in ion/drug transport, organic acid and lipid metabolic processes, while the expression of previously identified targets upon *Hnf1b*-ablation, including cystic disease genes was weakly or not affected. Postnatal analyses revealed renal abnormalities, ranging from glomerular cysts to hydronephrosis and rarely multicystic dysplasia. Urinary proteomics uncovered a particular profile predictive of progressive decline in kidney function and fibrosis, and displayed common features with a recently reported urine proteome in a RCAD pediatric cohort. Altogether our results show that HNF1B reduced levels lead to developmental disease phenotypes associated with the deregulation of a subset of its targets. They further suggest that this model represents a unique clinical/pathological viable model of the RCAD disease.

Key words: HNF1B transcription factor, RCAD syndrome, gene-dosage, glomerular and proximal tubule cysts, mouse models, transcriptomics

SUMMARY STATEMENTS

A novel established mouse model carrying a heterozygous splicing human mutation in the *Hnf1b* gene exhibits phenotypes similar to patients with the Renal Cysts and Diabetes disease.

INTRODUCTION

The transcription factor HNF1B is an important regulator of early mouse kidney, liver and pancreas organogenesis (Coffinier et al., 2002; De Vas et al., 2015; Gresh et al., 2004; Haumaitre et al., 2005; Heliot et al., 2013; Lokmane et al., 2008; Lokmane et al., 2010; Massa et al., 2013). Heterozygous mutations in the *HNF1B* gene are the cause of a complex human syndrome, known as Renal Cysts and Diabetes (RCAD, OMIM #137920) characterized by early onset of diabetes and developmental abnormalities of the kidney, genital tract and pancreas, as well as a variety of renal, liver, pancreas and biliary dysfunctions (Clissold et al., 2015) (Barbacci et al., 2004; Bellanne-Chantelot et al., 2004; Bellanne-Chantelot et al., 2005; Haldorsen et al., 2008; Haumaitre et al., 2006; Kettunen et al., 2017; Lindner et al., 1999).

More than one hundred fifty *HNF1B* heterozygous mutations have been described, including missense, nonsense, insertion/deletions, frameshift and splice site mutations as well as whole gene deletions (Alvelos et al., 2015; Barbacci et al., 2004; Bellanne-Chantelot et al., 2004; Chen et al., 2010; Edghill et al., 2006; Heidet et al., 2010). These mutations are either familial or de novo (40%). Intragenic mutations map predominantly in the DNA binding domain (exons 2 and 4), while whole gene deletions (1.3 Mb deletion at chromosome 17q12) account for up to 50% of the *HNF1B* variants. *HNF1B* mutant carriers exhibit a highly variable phenotype, both between and within families. No clear genotype-phenotype correlations were observed neither for the type or location of mutations, and haploinsufficiency has been the main underlying disease proposed mechanism.

The most consistent clinical feature associated with heterozygous *HNF1B*-mutations is severe non-diabetic renal disease. *HNF1B* mutations are also the most common monogenic causes of developmental kidney disease being part of a spectrum of malformations known as congenital anomalies of the kidney and urinary tract (CAKUT) (Nakayama et al., 2010) and Autosomal Dominant Tubule Interstitial Kidney Diseases (ADTKD) (Devuyst et al., 2019). A large spectrum of renal abnormalities have been reported, including unilateral or bilateral cysts, multicystic dysplasia, oligomeganonephronia, hypoplastic Glomerulocystic Kidney Disease

(GCKD), solitary kidney, and various dysfunctions (Chen et al., 2010; Clissold et al., 2015; Ferre and Igarashi, 2018; Shao et al., 2020).

The molecular mechanisms by which heterozygous mutations in *HNF1B* cause this broad spectrum of clinical symptoms remain poorly understood. Unlike humans, heterozygous mice for an *Hnf1b* null allele have no apparent phenotype, while the homozygous deletion results in early embryonic death (Barbacci et al., 1999). Constitutive inactivation of *Hnf1b* in the mouse epiblast (Haumaitre et al., 2005; Lokmane et al., 2008; Lokmane et al., 2010) or specific inactivation of *Hnf1b* either in renal tubules, liver or pancreas (Coffinier et al., 2002; De Vas et al., 2015; Desgrange et al., 2017; Gresh et al., 2004; Heliot et al., 2013) results in early embryonic or perinatal death along with far more severe phenotypes than those observed in the context of the RCAD disease.

During renal development, *Hnf1b* has been shown to be required for early ureteric bud branching and the induction of nephrogenesis (Lokmane et al., 2010). Specific deletion either in nephron progenitors or in collecting ducts uncovered additional later functions in early nephron segmentation (Heliot et al., 2013; Massa et al., 2013) and normal patterning and epithelial organization of collecting ducts (Desgrange et al., 2017). Additionally, *Hnf1b* deletion in medullar tubules at relatively later stages resulted in cystic kidneys after birth and downregulation of several cystic disease genes, including the HNF1B direct targets *Pkhd1*, *Pkd2*, *Kif12* and *Umod* (Gresh et al., 2004; Hiesberger et al., 2005). These findings led to the hypothesis that the renal phenotype in *HNF1B* mutant carriers could be attributed to the global inhibition of these cystic genes. However, analyses of fetuses carrying two different *HNF1B* mutations (Haumaitre et al., 2006) as well as of adult mutant carriers (Faguer et al., 2012) show that the cystic renal phenotype was not associated with decreased expression of the cystic disease genes identified in mice, implying that a more complex HNF1B transcriptional network underlies the human disease.

The genetic discrepancies between mouse models and human disease further suggest that mouse mutant models generated so far do not correctly represent the human mutations or alternatively mice are less sensitive to haploinsufficiency.

To explore these possibilities and obtain a more comprehensive view of HNF1B function in organ development and disease in the context of the whole animal, we generated a novel RCAD mouse model by introducing a previously identified human hotspot mutation at the intron-2 splice donor site (<IVS2nt+1G>T) (Bingham et al.,

2003; Harries et al., 2004). Moreover, since patients with these mutations exhibited the typical features of *HNF1B* mutations (Bingham et al., 2003), this model could be representative of a large number of *HNF1B* intragenic disease-causing mutations.

Characterization of the renal phenotype showed that mouse heterozygous mutants (referred as splicing mutation intron-2 (Sp2) *Hnf1b*^{Sp2/+}) exhibited bilateral cysts and tubular dilatations as well as glomerular cysts from E15, along with rare cases of genital tract abnormalities and extra renal manifestations similar to those described in human *HNF1B* mutant carriers. Unlike previous heterozygous mouse mutants for a null allele, in which the HNF1B protein levels remained either unchanged or even increased (Kornfeld et al., 2013), the HNF1B protein levels of *Hnf1b*^{Sp2/+} heterozygous mutants were reduced by 30 to 40%.

Transcriptional profiling analyses indicate that only a subset of the HNF1B target genes expressed primarily in early and mature proximal tubules was sensitive to reduced HNF1B levels at different embryonic stages, whereas the previously identified targets upon *Hnf1b* ablation were relatively insensitive. Postnatal analyses revealed several renal abnormalities ranging from few clusters of glomerular cysts and micro cysts to hydronephrosis and rarely multicystic dysplasia. Further urine proteomic analyses uncovered a particular signature of differentially excreted peptides in *Hnf1b*^{Sp2/+} mice exhibiting several similarities to the urinary peptide signature reported in pediatric RCAD patients (Ricci et al., 2019).

Our results highlight that reduced *Hnf1b* dosage in this mouse model differentially affects the expression of target genes leading to the onset of disease phenotypes.

RESULTS

Generation of a mouse model reproducing a human *HNF1B* splicing mutation

A mouse model carrying a point mutation at the intron-2 splice donor site, was generated by homologous recombination by introducing a G to T point mutation (Supplementary Fig.S1A) thus reproducing the c.544+1G>T (<IVS2nt+1G>T) human mutation (Bingham et al., 2003). The resulting *Hnf1b* mutated allele encompassed the human splicing point mutation and a unique LoxP-site within intron-1.

To define the consequences of this mutation on *Hnf1b* mRNA processing, we initially performed semiquantitative RT-PCR using RNA from *Hnf1b*^{Sp2/+} heterozygotes and wild-type (*WT*) kidneys and primers located in exon-1 and exon-3.

Sequence of the PCR products in *Hnf1b*^{Sp2/+} mutants indicated the production of the two expected *Hnf1b* spliced isoforms A and B and four additional novel transcripts, present at low levels, corresponding to the isoforms A and B in which were deleted either the exon 2 or the last 32 base pairs (bp) of exon 2 through the activation of a near cryptic splice donor site (Fig. S1B; see Material and Methods). The same pattern of alternative splicing in *Hnf1b*^{Sp2/+} heterozygous was observed at different stages (not shown).

Notably, previous mRNA analysis has shown that the human splicing mutations IVS2nt+2insT and IVS2nt+1G>T also resulted in exon-2 skipping. However, despite the conservation of the exon-2 cryptic splice donor site in humans (Fig.S1C), variants lacking the last 32 bp of exon-2 have not been described (Harries et al., 2004).

The predicted consequences of deleting either the entire or part of exon-2 are the generation of a frameshift leading to premature stop codons deleting the DNA binding domain and the entire C-terminal transactivation domain. This indicated that the spliced mutant transcripts are expected to generate non-functional proteins.

We subsequently examined the levels of *Hnf1b* transcript and protein produced by the normal allele in *Hnf1b*^{Sp2/+} heterozygous mutants and *WT* littermates, and searched for the presence of putative truncated proteins produced by the mutant allele.

Hnf1b-transcript levels were examined by quantitative real time PCR (qRT-PCR) using primers located in the ATG translational site and the last 32bp of the exon-2, thus allowing the detection of transcripts produced only by the normal *Hnf1b* allele (Table S2). We found that in *Hnf1b*^{Sp2/+}, the *Hnf1b* transcripts were significantly decreased by 30 to 42% relative to *WT* levels, in particular during embryonic stages. In adults, the reduction in transcript levels was highly variable and modest without reaching significance (Fig. 1A).

To examine the HNF1B proteins produced by both the normal and mutant allele in *Hnf1b*^{Sp2/+} heterozygous, we performed Western-blot analyses using whole cell extracts from microdissected kidneys of several independent embryo litters or adult mice and HNF1B antibodies raised against residues located within the first exon. As controls, we used extracts from transfected cells with expression vectors of either full-length HNF1B variant-A or the putative truncated proteins encoded by spliced mutant transcripts.

These analyses showed the lack of any detectable truncated protein encoded by abnormally *Hnf1b* spliced transcripts at any stage examined and even upon increasing 4-fold the concentration of extracts, under conditions where the truncated spliced versions expressed in transfected cells were easily detected (Fig. S2 A-C, E). Thus, these truncated proteins are either very unstable or not produced as previously described in several dominant mutations associated with premature termination codons (PTCs) (see below Discussion). Unlike previously characterized heterozygous mutants, we found a significant decrease in HNF1B protein levels in the *Hnf1b*^{Sp2/+} mutants, not only at embryonic stages but also in adults (Fig. 1B), further suggesting a posttranscriptional and/or translational control of HNF1B in postnatal life. By contrast and consistent with the absence of phenotype, we confirmed that in *Hnf1b*^{Lacz/+} heterozygous mice, HNF1B protein levels were significantly increased (Kornfeld et al., 2013)(Fig. 1C).

To acquire a detailed spatial pattern of HNF1B expression in heterozygous mutants we performed immunostainings at different embryonic stages. As compared to *WT*, *Hnf1b*^{Sp2/+} mutants exhibited from E15.5 a global reduction of the structures positive for HNF1B together with an unequal decrease in nuclear staining in several regions (highlighted in Fig. 1D insets). Dilated tubules did still exhibit nuclear staining (Fig. 1D).

In conclusion, these results show that the splicing mutation results in a loss of function allele together with decreased levels of the functional HNF1B protein as compared with *WT* levels. Notably, HNF1B protein is not decreased homogeneously in expressing structures, suggesting that these variations occur stochastically and underlie the heterogeneity in the disease phenotype.

***Hnf1b*^{Sp2/+} heterozygous mutant embryos exhibit bilateral glomerular cysts, tubular dilatations and hydronephrosis with variable severity depending on the genetic background**

To assess the onset and progression of the renal phenotype, we performed histological analyses of heterozygous mutants and *WT* littermates at different embryonic stages initially in a C57BL/6N x 129/sv mixed background (F1). Up to E14.5, heterozygous embryos developed apparently normally (Fig. S3A), although in some cases mutant embryo kidneys exhibited dilated Bowman's capsules (not shown). Subsequently from E15.5, we reproducibly observed bilateral cysts,

including glomerular and tubular cysts in the cortico-medullar regions (Fig. 2A-C). As kidney growth progressed, from E17.5 there was an apparent reduction of the volume of cystic structures relative to whole kidney volume, but glomerular cyst exhibited a rather similar distribution throughout development (Fig. 2D-F).

We then examined the influence of mouse strain susceptibility on the disease phenotype by backcrossing the *Hnf1b*^{Sp2/+} mutant mice into two inbred backgrounds: C57BL/6N and 129/sv. As observed in the mixed background, mutant kidneys in these two backgrounds exhibited tubular dilatations and glomerular cysts from E15.5 (Fig. 2G-N) and a more severe renal phenotype at embryonic stages than in postnatal life. However, in the C57BL/6N background the *Hnf1b*^{Sp2/+} embryonic kidneys presented a relatively more severe and variable phenotype, particularly at later stages and in newborn pups with higher numbers of both medullar and glomerular cyst, frequent unilateral or bilateral pelvic dilatations and hydronephrosis and more rarely duplicated kidneys (Fig. 2, Fig. S4). A summary of histological renal phenotypes observed from E18.5 to P0 is shown in Table S1A.

Heterozygous mutant embryos or newborns were obtained at the expected Mendelian ratio in different backgrounds. However, in the C57BL/6N background 10-15% of heterozygous mutants die between P1-25 days of age (Table S1B). Heterozygous mutants in both backgrounds were able to reproduce, but they were less fertile than *WT* littermates. Further postnatal analysis revealed rare cases of genital tract abnormalities (agenesis of the uterine horn, epididymis cysts, abnormal branched and highly dilated seminal vesicles) in either C57BL/6N or 129/sv backgrounds (not shown). Heterozygous mutants exhibited also several pancreatic dysfunctions including glucose intolerance and pancreatitis, a phenotype that will be described elsewhere (Quilichini et al., in press). Unless otherwise indicated, subsequent analyses were performed either in a mixed or in the C57BL/6N background.

These data show that *Hnf1b*^{Sp2/+} heterozygous mutants exhibited several of the urogenital phenotypes described in *HNF1B* mutant carriers. They also suggest that genetic modifiers may either aggravate (C57BL/6N) or attenuate (129/sv) the phenotype further contributing to variability in phenotypic manifestations.

***Hnf1b*^{Sp2/+} embryos display early proximal tubule dilations together with delayed differentiation of proximal tubules**

Hnf1b is known to be required for early ureteric bud branching and initiation of nephrogenesis (Lokmane et al., 2010). However, in *Hnf1b*^{Sp2/+} mutants neither early UB branching nor the expression of the early targets identified upon *Hnf1b*-ablation were affected (Fig. S3B). Notably the expression of Pax2, whose transcription in the collecting system depends on *Hnf1b* (Desgrange et al., 2017; Lokmane et al., 2010; Paces-Fessy et al., 2012) was not affected in *Hnf1b*^{Sp2/+} embryos neither at E14.5 or E15.5 (Fig. S3; Fig. 3A, A'), nor at later stages (data not shown). Nascent nephrons appeared normally induced as indicated by the presence of normally shaped Comma- and S-shaped bodies (Fig. S3B) and WT1 stained glomerular podocytes (Fig. 3D, D'). Although normally expressed both in the condensed mesenchyme around the ureteric buds and podocytes, WT1 expression was disrupted in glomeruli with dilated Bowman Capsules or cystic (Fig. 3D'; see below Fig. 4).

We then examined the origin of cystic/dilated tubular structures by staining with different nephron and collecting ducts markers from E15.5/E16.5 (Fig. 3) to E17.5 and P0 (Fig. S5). Mutant kidneys without overt hydronephrosis were examined to visualize the collecting duct network and medullar nephron tubules. The expression of HNF4A, a marker of early proximal tubules (PTs) and a target of HNF1B (Heliot et al., 2013) was heterogeneously and severely decreased both at E15.5 and E16.5 (Fig. 3E', G'; see also Figs S5 and S8) suggesting defective differentiation of PTs. Notably, HNF4A staining, which correlated with the reduced levels of HNF1B (compare Fig. 3C', D'), uncovered that a fraction of PTs were highly dilated, particularly at E15.5.

The expression of HNF1A, restricted to mature PTs, was similarly reduced at E16.5 (Fig. 3B'). Its expression was completely restored by E17.5 (data not shown), in contrast to HNF4A expression that showed only a partial restoration at E17.5 (Fig. S5A') or P0 (Fig. S5F'). Consistent with these observations, the mature PT marker LTA was not expressed up to the E16.5 stage (Fig. 3F') and began to be expressed by E17.5 (Fig. S5B'). Yet *Hnf1b*^{Sp2/+} PT clusters LTA+ both at E17.5 and P0 exhibited an unequal distribution and remained reduced in size (Fig. S5B', G').

Interestingly, the Na-K-Cl-cotransporter (NKCC2), expressed in the thick ascending limb of the loop of Henle (TAL), stained most of *Hnf1b*^{Sp2/+} medullar cysts

and tubular dilatations at E17.5 and P0 (Fig. S5C', H'). Distal tubules labeled by SLC12a3 (NCC) showed only rare and mild dilatations (data not shown).

Hnf1b^{Sp2/+} collecting ducts, stained either by AQP2 (Fig. S5D', I') or pancytokeratin (CK) (Fig. S5E'), were mainly devoid of dilatations. Intriguingly, they were not stained by the lectin DBA, neither during development nor in postnatal life (Figs. 3H'; S5J') uncovering impaired polarization of glycoconjugates in mutant collecting duct cells. This observation evoked an altered differentiation status of collecting duct cells, since previous studies have shown that UB cells begin to express DBA-binding glycoconjugates once they differentiate into stalks (Michael et al., 2007).

Thus, in addition to glomerular cysts, *Hnf1b*^{Sp2/+} heterozygous mutants display tubular cysts and dilatations that predominate initially in early PTs and subsequently from E17.5 in the TAL of Loop of Henle. Collecting ducts appeared morphologically normal but failed to express DBA-binding glycoconjugates.

Glomerular cysts display abnormal glomerulotubular insertion in *Hnf1b*^{Sp2/+} developing kidneys

Reminiscent of the glomerulocystic kidney disease described in *HNF1B* human mutant carriers (Bingham et al., 2001), glomerular cysts observed from E15 throughout development are the most common and earliest feature of the renal phenotype of *Hnf1b*^{Sp2/+}. It has been proposed that glomerular cystogenesis could secondarily result from transient obstruction of the urinary tract or developing nephrons or from defects in the junction of the PTs to the glomeruli (glomerulotubule junction) (Lennerz et al., 2010).

Without evidences of urinary tract obstruction, we further examined HNF1B, HNF4A and WT1 immunostainings on serial embryonic sections focusing on glomeruli with different degrees of Bowman's capsule expansion. We reproducibly observed that cystic glomeruli were surrounded by a decreased number of PTs often dilated or cystic (Fig. 4 compare A, B with D, E, G, H). Additionally, HNF4A and HNF1B staining showed that the glomerulotubular junction was laterally inserted into the Bowman's capsule and exhibited an unequal disorganized expression of HNF4A (Fig. 4H). Immunodetection of WT1 showed that the layer of podocytes of developing glomeruli with expanded Bowman's capsules become progressively disorganized, whereas *Hnf1b*^{Sp2/+} non-cystic glomeruli displayed the normal layer of podocytes (Fig.

4F, I). In more advanced glomerular cysts the expression of WT1 was lost (not shown).

Analysis of two *HNF1B* human mutant fetuses showing a very severe cystic renal phenotype (Haumaitre et al., 2006) also exhibited glomerulotubule junction defects Fig. 4M, N (R112fs, 27-weeks), O, P (P472fs, 31.5-weeks). They also presented separated tufts into 2 to 5, while in *Hnf1b*^{Sp2/+} tufts were separated in 2-3 or not separated (Fig. 4J-L).

These data together suggest that glomerular cysts in *Hnf1b*^{Sp2/+} result very likely from early defects in PT differentiation affecting the glomerulotubule insertion and leading to the accumulation of glomerular filtrate with subsequent expansion of the Bowman's space.

***Hnf1b*^{Sp2/+} cysts and tubular dilatations of developing nephrons are associated with defects in nephron differentiation and apico-basal polarity**

Cystogenesis in embryonic kidneys has been reported to be associated with several cellular defects, including abnormal cell-polarity, primary cilia defects, changes in cell-cell and cell-matrix interactions, as well as increased proliferation and apoptosis (Wilson, 2011). We found that the PT brush border marker Villin was normally expressed in *Hnf1b*^{Sp2/+} non-dilated tubules, but it was interrupted in cystic PTs (Fig. 5A-F). Cystic PTs also exhibited a stronger decrease in HNF4A expression (compare Fig. 5A, B, C). The expression of HNF1B was also moderately decreased in these dilated PTs as compared to its expression in other renal tubules (Fig. 5D, E, F).

Staining with α -acetylated tubulin to visualize cilia showed that the number of cells with cilium lining nondilated *Hnf1b*^{Sp2/+} collecting ducts or nephron tubules was not significantly different to that of *WT* embryos. However, we observed fewer cells with cilia in cystic and dilated PTs in comparison to non-dilated PTs (Fig. 5 H, I).

Interestingly, the basal membrane marker Laminin (Lam) exhibited a global decrease and partial disorganization in E15.5 heterozygous kidneys both in dilated and nondilated tubules (Fig. 5K, M). In medullar cystic tubules, the NKCC2 apical staining of epithelial cells of the thick ascending limb (TAL) of the Loop of Henle was also decreased in a proximo-distal gradient and disorganized (Fig. 5O,Q), while the apical markers of collecting ducts Muc1 and CK, were both correctly expressed (Fig.5 J, K, P, Q).

Further analysis of proliferation, using the mitosis marker phosphorylated histone H3, showed comparable numbers of proliferating cells in E14.5 renal tubular of heterozygous mutants and *WT* (not shown). However, at later stages the number of proliferating cells in *Hnf1b*^{Sp2/+} normal tubular structures exhibited an increase of 1,84-fold relative to *WT* tubules. Consistent with the enhanced proliferation associated to cystic expansion in ADPKD (Hopp et al., 2012), a higher and significant increase of proliferating cells was observed in *Hnf1b*^{Sp2/+} dilated/cystic tubules relative to *Hnf1b*^{Sp2/+} non-dilated normal tubules (Fig. S6). No changes were observed in the number of apoptotic cells assessed by TUNEL (not shown).

Together these results show that decreased levels of HNF1B appear to affect basal membrane organization without affecting apical cell polarity markers in non-dilated tubules. Moreover, proliferation was increased in cystic tubules relative nondilated tubules and even nondilated tubules exhibited increased proliferation compared with *WT*. The decreased expression of apical and brush border markers as well as the decreased number of cilia observed in *Hnf1b*^{Sp2/+} cystic tubules appear to be secondary to tubular dilatations.

Transcriptomic analyses of heterozygous mutant kidneys during development uncover variable dosage sensitivity among *Hnf1b* targets

To further elucidate the cellular and molecular components sensitive to HNF1B levels, we performed RNA-sequencing on *WT* and heterozygous mutant kidneys at E14.5 (considered histologically as pre-disease kidneys) and at disease stages (E15.5, E17.5 and P1) as detailed in Material and Methods.

Since heterozygous mutants still expressed HNF1B, we considered an absolute fold-change cutoff value of $>$ or $<$ 0.5 log₂FC, with an adjusted p-value $<$ 0.05. Remarkably, several genes were differentially expressed with Log₂FC $>$ -1 at all stages (Table S3), while only a few up-regulated genes differentially expressed were detected. We found an increased number of downregulated genes from E14.5 up to E17.5 followed by a partial decrease at P1, in agreement with a partial restoration of several PT markers expression. Accordingly, the numbers of downregulated genes shared between stages increased to reach 107 genes between E17.5 and P1 (Fig.6; Table S3, File 5).

Down-regulated genes with greater fold-changes were predominantly expressed in early and maturing PTs and to a lesser extent in primitive Loops of Henle and distal tubules (Table S3, file 6). At E17.5 and P1, downregulated genes included drug-metabolizing enzymes (*Abcc2*, *Ggt1*, *Fmo2*, *Akr1c1*) and more than fifty SLC-transmembrane-transporter genes (organic cation, sodium glucose, sodium phosphate transporters; Table S3, Files 7, 8).

GO-term analyses (Chen et al., 2009) highlighted transporter activity, active trans-membrane transporter activity, organic acid and lipid metabolic processes and metabolism terms as well as an association with abnormal renal/urinary system physiology, renal reabsorption, aminoaciduria and decreased urine osmolality. From E17.5 and consistent with the onset of mature cell-types in the developing nephrons, the pathways enriched included SLC-active transmembrane transport (transport of glucose and small molecules and metabolism) (Fig.6; Table S4).

The regulatory sequences of most downregulated genes contained HNF1 consensus binding sites. Consistently, specific HNF1B recruitment to the regulatory sequences of many of them has been reported by ChIP-PCR or ChIP sequencing (reviewed by (Ferre and Igarashi, 2018) and (Shao et al., 2020)). Amongst those targets strongly downregulated at most stages were *Hnf4a*, *Tmem27*, *Cubn*, *Spp1*, *Spp2*, *Pah*, *Kcnj*, *Pdzk1* and several SLC-transmembrane transporters, representing the subset of targets that appeared particularly sensitive to reduced HNF1B protein levels (Table S3). Interestingly, many of the genes downregulated at E17.5/P1 and regulated by HNF1B, were also found strongly decreased in *Hnf4a* mutant P1 kidneys (Marable et al., 2020)(Table S3, File 8). By contrast, the expression of previously identified targets strongly reduced upon *Hnf1b* ablation, including *Wnt9b*, *Pax2*, *Pkd2*, *Bicc*, *Tg737*, *Crb3*, *Kif12*, *Cys1*, *Glis2*, *Glis3*, were either modestly decreased or not affected. These results were further validated by q-RT-PCR (Fig. S7, Table S3). Interestingly, the well-known targets *Umod*, *Tmem27* and *Pkhd1* (Gresh et al., 2004) were found significantly downregulated at E17.5, but not at P1 (Table S3).

RNA-seq data was further validated by in situ hybridization (ISH), immunostaining and additional q-RT-PCR analyses. ISH of *Fbp1* and *Spp2*, two early PT anchor genes (Thiagarajan et al., 2011) revealed a strong downregulation in *Hnf1b*^{Sp2/+} kidneys of *Fbp1* transcripts and to a lesser degree of *Spp2* both at E17.5

and P0 (Fig. S7). Likewise, immunofluorescence analysis of E17.5 and P0 *Hnf1b*^{Sp2/+} kidneys showed strong reductions of TMEM27, SPP1 and CUBN staining and a more modest decrease of LRP2 (Fig. 7 A-D').

Q-RTPCR analysis indicated that the early PT markers *Hnf4a*, *Lrp2*, *Cubn*, *Tmem27* and the Loop of Henle markers *Kcnj1* (*RomK*) and *Umod* were preferentially downregulated during development up to P0 (Fig. 7E). Additionally, *Aqp2*, a gene downregulated in developing collecting ducts lacking *Hnf1b* (Desgrange et al., 2017) and upregulated in postnatal kidneys of *Hnf1b*-conditional inactivated medullar renal tubules (Gresh et al., 2004), was also found to be downregulated throughout development and progressively increased in *Hnf1b*^{Sp2/+} adult kidneys (Fig. 7E).

Remarkably, the expression of *Hnf1a* expressed later than *Hnf1b* and restricted to developing and adult PTs, was only moderately decreased at E15.5 and remained comparable to *WT* levels at P0 and in postnatal mutant kidneys (Fig. 7E). Thus, HNF1A, which has the same DNA recognition sequence that HNF1B and binds DNA as homo- or heterodimers with HNF1B, was apparently unable to compensate for HNF1B reduced levels during development. Conversely, *Hnf1a*^{-/-} adult mice exhibited a severe dysfunction of PTs together with strongly reduced *Lrp2* and *Cubn* expression, despite the increased expression of *Hnf1b* (Terry et al., 2016). These observations together, suggest distinct and sequential functions of HNF1B and HNF1A in developing versus adult PTs. Consistent with this hypothesis, we found that, in sharp contrast to our *Hnf1b*^{Sp2/+} mutants, E16.5-E17 *Hnf1a* null kidneys exhibit normal PT expression of CUBN, LRP2, HNF4A, HNF1B and LTA and the absence of an embryonic renal phenotype (Fig. S8).

Thus, among the various metanephric kidney developmental processes known to be controlled by HNF1B, the genes participating to early PT differentiation and nephron segment maturation (PT, loop of Henle) are those exhibiting a unique response to HNF1B protein dosage, highlighting a differential dosage-sensitivity of HNF1B-activated genes during kidney development. Amongst these targets, *Hnf4a* has been shown to play an important role in PT maturation and function, by direct regulation of many genes involved in transmembrane transport and metabolic processes (Marable et al., 2020) which are also transcriptionally regulated by *Hnf1b* (Fig. 6, Table S3-File 8). Moreover, our results suggest that a fraction of PT genes, including *Lrp2*, *Cubn* and *Sglt2* in postnatal life become controlled primarily by

HNF1A (Terry et al., 2016), thus replacing at least in part the critical role of HNF1B during embryogenesis.

Preliminary postnatal characterization of heterozygous *Hnf1b*^{Sp2/+} mutant mice

As mentioned above (Table S1B), a fraction of heterozygous died between P1 and P25. Otherwise, mice lived more than one year, beginning to manifest disease symptoms, albeit with variability, approximately from 8-10 months. Further histological analysis of adult *Hnf1b*^{Sp2/+} mice revealed variability in the severity of the renal phenotype with increased abnormalities observed both in aged males and females. They usually exhibited unilateral hydronephrosis while the other kidney was less affected, displaying mainly cortical or medullar glomerular cysts with collapsed or rudimentary capillary tufts (Fig.S9, B, C, H, I) as well as microcysts (Fig.S9 B, I). Dilated Bowman's spaces were often filled with finely granular proteinaceous material (Fig. S9 B', C, E', I'). A rare case (1/48 heterozygous mutants) exhibited bilateral severely affected kidneys: one kidney was highly dysplastic/hypoplastic and the other severely hydronephrotic (Fig. S10H, H'), indicating progressive hydronephrosis with age. Accordingly, some old mice (males or females) developed giant hydronephrosis (Table S5A).

Body weight curve analyses showed approximately 20% reduction in weight of heterozygous mice relative to *WT*, with males and females behaving rather similarly, while kidney weight/body weight ratio of males at different ages did not show significant differences as compared to *WT* littermates (Fig. S10, Table S5B).

Urinary analyses at different ages under basal conditions indicated that while 3-month-old *Hnf1b*^{Sp2/+} mutant mice exhibited normal physiological parameters, 6 month-old mice displayed defective urine concentrating ability with polyuria, and reduced urine osmolality (Table 1). Reduced urine osmolality was also observed after 22hs of water deprivation (data not shown). By 12-months, although urine volumes remained higher than *WT*, urine osmolality was more modestly and non-significantly decreased (Table 1). A similar increase in 24-hour urine output and daily water consumed was observed in three independent groups of 5-6-months mutant mice, followed by an attenuation of these parameters in 12-month-old mice (Table S5C). Impaired urinary concentration ability was also observed in 8-months *Hnf1b*^{Sp2/+} mice in a mixed genetic background, but not in the 129/sv background (not shown).

Consistent with the lower urine osmolality, 6-month-old *Hnf1b*^{Sp2/+} mice had significantly lower urinary magnesium, sodium and potassium concentrations, while the total excretion of these solutes was increased as compared to *WT* (Table 1), a tendency maintained in 12-month-old mice, although did not reach significance. Interestingly, urinary calcium concentration was significantly increased despite decreased osmolality. Moreover, plasma analysis in a separate group of mice revealed an increase of creatinine levels, although non-significant, while the levels of Mg were similar to *WT*. A significant increase in the levels of the alanine aminotransferase ALT and a tendency of higher levels aspartate aminotransferase (AST) were observed, reflecting potential liver dysfunctions in heterozygous mutant mice, as reported in some RCAD patients (Iwasaki et al., 1998).

To gain further insight into the pathophysiology of the renal disease we performed low molecular weight urinary proteome analyses from 17 *Hnf1b*^{Sp2/+} mutant and 18 *WT* mice (age ranging from 3-months to 17-months), using capillary electrophoresis coupled to mass spectrometry (CE-MS) and tandem mass spectrometry (MS/MS). We identified 40 significant differentially excreted peptides. The most prominent findings associated with our mutants were a substantial decrease of Epidermal Growth Factor (EGF), uromodulin and the kidney androgen-regulated protein (KAP) as well as a tendency of an increase of collagen protein fragments in the urinary excretion (Table S6). Interestingly, increased collagen peptides and decreased uromodulin levels were also observed in the urinary proteome of a pediatric cohort of RCAD patients (Ricci et al., 2019). Increased excretion of collagen fragments are consistent with the active extracellular matrix (ECM) remodeling that has been related to ECM modifications observed during cyst expansion (Wilson, 2011), while reduced urine uromodulin excretion has been associated with diminished markers of renal tubular function. Particularly, uromodulin, expressed exclusively by the epithelial cells lining the TAL, is excreted into the urine by proteolytic cleavage. The processing and release of uromodulin by TAL cells was found to be regulated by two targets of HNF1B (Ferre and Igarashi, 2018), the potassium channel *Kcnj1* and the calcium sensing receptor *CaSr* both expressed in TAL cells (Devuyst et al., 2019). These observations suggest that decreased uromodulin excretion may reflect a global dysfunction of TAL cells both in our mutants and RCAD patients.

In conclusion, *Hnf1b*^{Sp2/+} adult mice exhibit progressive renal abnormalities associated with a tendency to defective urinary concentration ability under basal conditions, associated with increased excretion of certain solutes and hypercalciuria, followed by a partial recovery in old animals. Urinary proteome analysis uncovers a particular profile of our heterozygous mutants predictive of progressive decline in kidney function and kidney injury and exhibits common features to the recently reported urine proteome in a pediatric cohort of RCAD (Ricci et al., 2019).

DISCUSSION

We report here the generation and characterization of a novel mouse model of the RCAD disease by reproducing an identified human splicing mutation and show that several of the urogenital defects described in *HNF1B* mutant carriers are replicated at the heterozygous state. These observations confirm that mice are sensitive to haploinsufficiency for *Hnf1b*, further highlighting the importance of precisely replicate human disease mutations.

Although previously described *Hnf1b* mouse mutations (Barbacci et al., 1999; Coffinier et al., 1999) generated a loss of function allele similar to our new model, the levels of the HNF1B protein at the heterozygous state were not decreased but rather increased instead of decreasing (Kornfeld et al., 2013) (Fig. 1C). The underlying mechanism is not yet identified. By contrast, and as expected, in our heterozygous mutants the levels of both *Hnf1b* transcript and protein produced by the *WT* allele were significantly reduced during development. In postnatal life, mainly the levels of HNF1B protein remained reduced, but not those of transcripts suggesting that HNF1B activity may additionally be regulated at the post-transcriptional and/or translational level (Fig. 2A, B). Further studies are required to define how HNF1B protein levels or its activity are regulated. The ubiquitin-proteasome pathway and miRNA-mediated regulation of HNF1B are, amongst others, possible mechanisms mediating tightly regulation of HNF1B protein levels and potentially deregulated in our model. This knowledge will certainly have potential implications for disease therapy.

Although abnormal spliced transcripts are expressed at low levels (Fig. S1B), no evidence of nonsense-mediated mRNA decay (NMD) was observed (data not shown), thus confirming previous studies in human *HNF1B* mutations (Harries et al., 2005). Moreover, we did not detect any of the potential truncated proteins encoded

by these alternative spliced transcripts (Fig. S2) and we cannot exclude the fact that truncated proteins were rapidly degraded by the ubiquitin-mediated protein quality control system (Rousseau and Bertolotti, 2018). However, it is more likely that *Hnf1b*-mutant spliced transcripts not degraded by NMD, are not translated through a process known as NonsenseMediated-Translational-Repression (NMTR), a well-documented mechanism described in several frameshift mutations in cancer cells (You et al., 2007) as well as human dominant diseases associated to premature termination codons (PTCs) (Barefield et al., 2015; Rio Frio et al., 2008). Indeed, these different studies have shown that the products of mutant alleles containing PTCs are degraded or inactivated by two complementary mechanisms, NMD and NMTR effectively preventing the synthesis of truncated proteins and leading to null alleles and decreased amounts of functional proteins. In summary, these observations suggest that intragenic *HNF1B* mutations leading to PTCs, which represent more than 50% of intragenic mutations (Alvelos et al., 2015), very likely do not lead to the production of truncated proteins, further explaining the observed lack of genotype-phenotype correlations in RCAD patients.

The high variability in the phenotype of *HNF1B* mutant carriers has been explained by diverse mechanisms ranging from modifier genes, environmental factors to interacting cofactors. Our heterozygous mutants did develop heterogeneous urogenital abnormalities with a more severe phenotype in the C56BL//6N background than in the 129/sv background suggesting that genetic modifiers may indeed either aggravate or attenuate the disease phenotype. Remarkably, even in these two inbreed backgrounds we still observed variability in the phenotype presentation of *Hnf1b*^{Sp2/+}, notably at later developmental stages and postnatal life. In particular, in the C57BL/6N background often one kidney was more severely affected and hydronephrotic than the other. Unilateral affected kidneys have also been reported in RCAD patients (Chen et al., 2010; Heidet et al., 2010). This variability was also observed between *Hnf1b*^{Sp2/+} mutants even when they were from the same litter and raised together, in order to reduce environmental exposition variations. One possible mechanism underlying the phenotypic variability of our mutants and *HNF1B* mutant carriers could be the inherent stochasticity in transcription and translation processes (Bar-Even et al., 2006), together with the

known increased susceptibility to stochastic delays or interruptions of gene expression due to haploinsufficiency (Johnson et al., 2019).

Global transcriptional profiling indicates that only a subset of the established *Hnf1b* target genes primarily involved in early proximal tubule differentiation and onset of nephron tubule mature functions were sensitive to HNF1B reduced levels during development.

The HNF1B target gene *Hnf4a* (Heliot et al., 2013), involved in proximal tubule maturation and function (Marable et al., 2020; Martovetsky et al., 2013) is the major transcriptional regulator strongly reduced in our mutants at all developmental stages. Transcriptomic and CHIP-analyses have recently shown that HNF4A controls proximal tubule maturation via direct activation of transporter and metabolism genes (Marable et al., 2020). A large proportion of HNF4A-targets are also targets of HNF1B (Fig. 6, Table S3, File 8), further suggesting a shared function of HNF1B and HNF4A on developing PTs that relies on synergistic interactions between the two factors at common targets. Such a functional interdependence between HNF1A and HNF4A has already been described in pancreatic islets (Boj et al., 2010) and may explain an increased vulnerability to decreased *Hnf1b* gene-dosage. In this context, RNA analysis of renal tissue of a *HNF1B* patient carrying a point mutation showed a strong downregulation of *HNF4A*, *KIF12* and *PPARGC1A* as well as *HNF1B*, while other known HNF1 targets remained unchanged (Casemayou et al., 2017). This patient presented a generalized defect of proximal and distal tubular function, incomplete tubular acidosis, hypercalciuria and mitochondrial dysfunction. These observations together highlight the recurrent role of *HNF1B* in PT cells and disease also in adulthood.

Several of the PT genes strongly downregulated during development in our mutants have additionally been shown to be targets of HNF1A or HNF1A/HNF1B heterodimers in adult kidneys (David-Silva et al., 2013; Kikuchi et al., 2007; Saji et al., 2008). In our mutants the expression of *Hnf1a* in the PT was only moderately decreased at E17.5 and not affected at P1 or adults (Fig. 7E, Table S3), suggesting that HNF1A was unable to compensate for HNF1B decreased levels during development. Accordingly, we found normal PT development and marker expression in *Hnf1a*-null embryo kidneys (Fig. S8). However, it appears, at least partially, to compensate in postnatal life as indicated the restoration of the expression of some PT markers such as *Lrp2* and *Spp2* in *Hnf1b*^{Sp2/+} adult kidneys. Moreover, adult

Hnf1b^{Sp2/+} mice did not show glycosuria, suggesting again that HNF1A replaced HNF1B in the control of *Sglt2* (*Slc5a2*), a gene strongly downregulated in our mutants at both E17.5 and P1. Note however that the renal expression of other known targets, including *Tmem27* and the cationic amino acid exchanger *Slc7a9* were found not affected in *Hnf1a*-deficient mice (Bonzo et al., 2010) and remained downregulated in our heterozygous mutants (Fig.7, Table S3), highlighting the complexity in the regulatory networks of these two transcription factors in the cells they coexpress.

The observed dynamic and temporal regulation patterns (i.e. some genes were strongly downregulated at an early stage but not at a later stage) suggest an increasing complexity in the regulatory network involved in the differentiation and maturation of nephron segments. It is tempting to speculate that similar changes in the promoter occupancy patterns during development involving new recruitments, release, and exchange of HNF1A and HNF1B as described during hepatocyte differentiation (Kyrmizi et al., 2006) take also place during renal development.

Similar to the human disease, glomerular cysts are the most common and earliest feature of the *Hnf1b*^{Sp2/+} embryonic renal phenotype. Although not expressed in glomeruli, HNF1B is expressed in the parietal cells of the Bowman's capsules, suggesting a potential implication in glomerulogenesis. It has been shown that glomerular cysts in *Col4a1* adult mutant mice were preceded by alterations of parietal epithelial cells that abnormally expressed CD44, α -SMA and claudin-1 (Chen et al., 2016). We have not observed such alterations in our mutants, although *claudin-1* expression appeared more disorganized relative to *WTs* (not shown). Detailed analysis of glomerular cysts of *Hnf1b*^{Sp2/+} embryonic kidneys exhibiting different degrees of Bowman's capsule expansion, suggest that glomerular cysts result very likely from delayed and/or abnormal differentiation of early PTs associated with an abnormal glomerulotubular insertion, thus leading to the accumulation of glomerular filtrate and the subsequent expansion of the Bowman's space and glomerular tuft atrophy. Notably, abnormal PT insertion into the Bowman Capsule was previously described in *Hnf1b*-conditional inactivated mutants in nephron progenitors (Heliot et al., 2013) and more recently further characterized through detailed imaging analyses uncovering in addition tubular obstruction (Fiorentino et al., 2020). Neither glomerular cysts nor PT dilatations were observed in *Hnf4a* mutant

mice (Marable et al., 2020), thus excluding that its decreased expression in our mutants is related to these phenotypes. These observations are consistent with the earlier and broader role of HNF1B in renal epithelial tubule morphogenesis.

In adulthood *Hnf1b*^{Sp2/+} mice exhibited defective urinary concentration ability under basal conditions and hypercalciuria until 6-month-old followed by a partial restoration by 12-month-old. Defects in urine concentration have recently been described in mice with specific *Hnf1b* inactivation in the collecting ducts at later stages, a phenotype that was associated with increased AQP2 expression and abnormal apical localization, downregulation of the urea transporter UT-A1 (*Slc22a12*) and the direct control of FXR (Aboudehen et al., 2017). Although further analyses are required, including urinary concentration ability under different conditions, it is interesting to note that we have also observed a progressive increase in *Aqp2* expression in adult *Hnf1b*^{Sp2/+} mice together with a downregulation of *Fxr* (*Nr1h4*) (Fig.7E). *Slc22a12* was also found downregulated at E17.5 and P1 (Table S3).

Adult *Hnf1b*^{Sp2/+} mice also exhibited unilateral hydronephrosis. Physical ureter obstruction, one of the most common causes of hydronephrosis, was not detected in our mutants. Occasionally we have observed dilated ureters at the ureteropelvic junction (Fig. S4-C57BL/6N). Hydronephrosis/hydroureter have been also described in RCAD patients (Adalat et al., 2009) as well as in different mouse models of *Hnf1b*-inactivated in the collecting ducts (Aboudehen et al., 2017; Desgrange et al., 2017). Further analyses are required to define whether hydronephrosis is due to the reported polyuria and defective osmoregulation (Aboudehen et al., 2017) or through the previously described perturbations in smooth muscle differentiation of the ureter (Paces-Fessy et al., 2012) or both. Of note, *Hnf4a* mutant mice exhibited at P14 overt non-obstructive hydronephrosis probably due to the lack of reabsorption in PTs (Marable et al., 2020). It is, therefore, possible that the observed developmental downregulation of *Hnf4a* contributes, at least in part, to the onset of this phenotype.

Metabolic profiling of different organs, including kidney, pancreas and liver as well as plasma of adult *Hnf1*^{Sp2/+} mice was previously reported (Torell et al., 2018). We found evidence of impaired amino acid renal metabolism and reduced plasma levels of total free amino acids and increased myo-inositol, which are metabolic parameters reflecting impaired renal function, together with disturbed hepatic

metabolism. Likewise, and as reported in RCAD mutant carriers, we observed in adult mutants a significant increase in the plasma of the alanine aminotransferase (ALT) levels and a tendency of higher levels of aspartate aminotransferase (AST), reflecting liver dysfunctions (Table 1). Unlike humans, adult mice did not exhibit hypo-magnesemia and/or hyper-magnesuria reported in more than 30% of *HNF1B* adult mutant patients. These results may reflect differences between mouse and humans in ion-transport regulation and/or adaptive mechanisms.

Notably, urinary proteome analysis uncovered a particular profile in our heterozygous mutants, with a substantial decrease of uromodulin and EGF peptides, predictive of progressive decline in kidney function, as well as increased collagen fragments, consistent with an excessive ECM turnover. Urinary proteome analysis in a pediatric cohort of RCAD patients revealed a similar signature with a majority of peptides collagen type I or type III fragments enriched in the urine of RCAD patients and a decrease of uromodulin fragments, together with other additional de-regulated peptides (Ricci et al., 2019). Altogether these observations emphasize a more global implication of HNF1B in postnatal kidney function in our mutants involving different nephron segments and collecting ducts and likely associated with a deregulation of additional identified target genes (reviewed by (Shao et al., 2020). Consistent with a role of HNF1B in postnatal tubular maintenance and transport activity, recent clinical data of a pediatric cohort of *HNF1B* mutant carriers show that abnormal tubular electrolyte handling develops progressively with age (Adalat et al., 2019).

Thus, our study shows how constitutive heterozygous germline mutations affect early kidney development and provides further insights into the mechanisms underlying the renal developmental abnormalities associated with RCAD and their consequences in postnatal life. In summary, the *Hnf1b*^{Sp2/+} mouse model represents a unique clinical/pathological viable model of the human disease and promises to be important in the integrative evaluation, in the context of the whole animal, of the broad facets of this disease ranging from various developmental abnormalities to kidney, pancreas and liver dysfunctions as well as tumorigenesis (Yu et al., 2015).

MATERIAL AND METHODS

Generation of a mouse model carrying a point mutation at the intron 2 splice donor site

The knock-in mouse carrying a human splicing point mutation was generated according to a proposal of S. Cereghini with the support of the GIS Maladies Rares and the Mouse Clinical Institute. The *WT* sequence GAC/g taagtgtttaacctt was mutated to GAC/t taagtgttta**agctt** sequence (Capital letters show end Exon2 bases, lower letters indicate the intron2-Exon2 junction sequence, in bold the point mutations). The splice mutation into the *Hnf1b* locus was introduced by homologous recombination into 129/sv ES cells. Two correctly recombined ES clones were obtained, which were additionally used to differentiate into embryoid bodies and confirm the generation of expected *Hnf1b* spliced transcripts before the generation of the mouse line. We additionally perform mRNA analysis of *Hnf1b*^{Sp2/+} ES differentiated into embryoid bodies in the presence of the NMD inhibitor cycloheximide (100 µg/ml, 5hs) as described (Barbacci et al., 1999) and found no alterations in the levels of alternative spliced transcripts (not shown). Chimeric mice were obtained by microinjection into C57BL/6N blastocysts. The *LoxP*-flanked neomycin-resistance cassette was located within intron-1 and subsequently excised by breeding heterozygous mutant mice with a “Cre deleter” mouse line. Thus, the mutated allele encompassed the point mutation at the splice donor site in addition to a single *LoxP* site and HindIII restriction site aagctt (underlined) within intron 2. Mice homozygous for the splicing mutation were lethal before gastrulation. The line was maintained as heterozygous either in a mixed C57BL/6N x129sv or in pure C57BL/6N and 129/sv backgrounds, in general by crossing heterozygous males with *WT* females. Whatever the background, we noticed that the relative severity of the renal phenotype of heterozygous mutants was higher in the descendants of crosses of heterozygous males and females. In addition to the renal phenotype mice in the C57BL/6N exhibited unilateral or bilateral absence of eyes (30% of n: 36 *Hnf1b*^{Sp2/+} males and n=20 *Hnf1b*^{Sp2/+} females) manifested from embryo stages. Intriguingly the same eye phenotype was observed in approximately 15% of heterozygous for a null allele (see EMMA description). This ocular phenotype remains undefined. It may be linked to the mutation Rd8 mutation of the *Crb1* gene present in the strain C57BL/6N

(Mattapallil et al., 2012). Yet, there is no evidence that is related to HNF1B dosage, since is present in the two heterozygous mutants *Hnf1b*^{Sp2/+} and *Hnf1b*^{lacZ/+}.

Mice heterozygous for the *Hnf1b* null allele (*Hnf1b*^{lacZ/+}; international designation: *Hnf1b*^{tm1Sce}, with the *lacZ* gene and the SV40 polyadenylation sequence and neomycin resistance cassette, replacing the first exon of *Hnf1b* (Barbacci et al., 1999), were maintained as heterozygotes. The mouse line in a pure 129/sv (129/sv-*Hnf1b*^{tm1Sce}) and C57BL/6N (C57BL/6N-*Hnf1b*^{tm1Sce}) backgrounds are available at EMMA (The European mouse mutant archive) (EMMA ID: EM:07817 and EM:07827, respectively) together with the phenotype description. The *Hnf1a*^{+/-} mice were provided by Frank Gonzalez (Laboratory of Metabolism, NCI/CCR) (Lee et al., 1998) and maintained as heterozygotes in the C57BL/6N background.

Animal care and the experimental protocols were approved by and conducted in accordance with French and European ethical legal guidelines and the local ethical committee for animal care (Comité d'éthique en Expérimentation Animale Charles Darwin N°5, approval number N° 04817.02), respecting the 3R rule.

Paraffin-included human fetal tissues were obtained from family members with informed consent approved by the Ethics committee of Debre´ Hospital (Anne-Lise Delezoide, Service de Foetopathologie, Hôpital Robert Debré, Paris, France), as previously reported in (Haumaitre et al., 2006).

In situ hybridization (ISH) and immunohistochemistry

In situ hybridization (ISH) on paraffin sections was performed as described (Lokmane et al., 2008). The *Fbp*, *Spp2* cRNA probes were generated by PCR (GUDMAP database). Embryos and postnatal kidneys up to 2-month-old were fixed with 60% ethanol/11% formaldehyde and 10% acetic acid. Adult kidneys (> 2-months) were fixed in alcoholic Bouin (Duboscq-Brasil) solution and paraffin sections were used for H&E histological analysis and immunohistochemistry. Antibody staining on paraffin sections was performed as described (Desgrange et al., 2017; Lokmane et al., 2010). For each probe (ISH) or antibody sections from at least three different embryos were used. The primary and secondary antibodies are listed in supplementary Table S7.

RNA extraction and real-time PCR analysis

Both kidneys of each embryo up to postnatal P1 were dissected in ice-cold Dulbecco Modified Medium (DMEM) and washed in ice-cold PBS. *WT* and heterozygous

mutant embryos were from the same litter. Adult kidneys were cut sagittal: one half was used for histology, ¼ w for RNA extraction and the other ¼ piece for protein extraction. Total RNA was extracted using the miRNeasy Mini Kit (Qiagen), Dnase1 treated on the columns and 250- 500 ng was reverse-transcribed using the High-capacity cDNA reverse transcription kit (Applied Biosystems). Real-time PCR was performed using Fast SYBR Green master mix (Applied Biosystems) and the Step-One Plus system (Applied Biosystems) described (Paces-Fessy et al., 2012). The primers used are listed in Supplementary Table S2. Number of kidney samples is indicated in the figures. The mean and SEM were calculated by genotypes and the statistical significance was determined using Student's t-test (significance at * $P < 0.05$, ** $P < 0.01$, *** $P < 0.001$).

Semiquantitative RT-PCR

Total RNA from microdissected kidneys was extracted and subjected to semiquantitative RT-PCR as described (Lokmane et al., 2008) with the following modifications. The conditions were chosen so the RNAs analyzed were in the exponential phase of amplification by performing different PCR cycles as indicated in Fig. S1. PCR products were resolved in 2% agarose/TBE ethidium bromide gels and photographed using GELDOC documentation system. Densitometry quantification was performed with ImageJ software. Primer sequences used were Gapdh for normalization and for *Hnf1b*, vATG and v695 (Table S2).

The cDNA sequence of spliced isoforms and the encoded truncated proteins from the mutated *Hnf1b* allele are:

1- SPLICED ISOFORM A/B Δ32bp EXON2

Underlined show retained exon2 minus 32bs

cDNA sequence

ATGGTGTCCAAGCTCACGTGCTCCAGCAAGAACTCCTGAGTGCCCTGCTGAGCTCCGGAGTCACCAA
GGAAGTGCTGATCCAGGCCTTGGAGGAGTTACTGCCGTCCCCGAATTTCGGGGTGAAGCTGGAGACAC
TGCCCTGTCCCCGGGAGCGGGGCGGATCTCGACACCAAGCCGGTTTTCCATACTCTCACCAATGGC
CACGCCAAGGGCCGCTTGTCTGGGGACGAGGGCTCAGAGGACGGCGACGACTATGACACTCCTCCCAT
CCTCAAAGAGCTCCAGGCGCTCAACACCGAGGAGGCCGCGGAGCAGCGGGCCGAGGTGGACCGGATGC
TCAGCGAGGACCCGTGGAGGGCTGCCAAAATGATCAAGGGATACATGCAACAGCACAATATCCCCAG
AGGGAGGTGGTTCGATGTCACAGGCCTGAACCAATCCCACCTCTCTCAACACCTCAACAAGGGCACCCC
CATGAAGACCCAGAAGAGAGCTGCCCTGTACT**TGA**g

Putative encoded protein (170 amino acids)

MVSKLTSLQQLLSALLSSGVTKEVLIQALELLPSPNFGVKLETLPSPGSGADLDTKPVFHTLTNG
HAKGRLSGDEGSEDGDDYDTPPIKELQALNTEEAEEQRAEVDRLSEDPWRAAKMIKGYMQQHNIPQ
REVVDTVTLNQLSHLSQHLNKGTPMKTQKRAALYT*VQPD

2- SPLICED ISOFORM A Δ EXON2

cDNA sequence (underlined show spliced exon 3)

ATGGTGTCCAAGCTCACGTCGCTCCAGCAAGAACTCCTGAGTGCCCTGCTGAGCTCCGGAGTCACCAA
GGAAGTGCTGATCCAGGCCTTGGAGGAGTTACTGCCGTCCCCGAATTTTCGGGGTGAAGCTGGAGACAC
TGCCCCGTGTCCCCCGGGAGCGGGGCGGATCTCGACACCAAGCCGGTTTTCCATACTCTCACCAATGGC
CACGCCAAGGGCCGCTTGTCTGGGGACGAGGGCTCAGAGGACGGCGACGACTATGACACTCCTCCCAT
CCTCAAAGAGCTCCAGGCGCTCAACACCGAGGAGGCCGCGGAGCAGCGGGCCGAGGTGGACCGGATGC
TCAGAGTTCAACCAGACAGTCCAGAGCTCTGGAAACATGACAGACAAAAGCAGTCAGGATCAGCTGCT
GTTTTCTTTCCAGAGTTCAGTCAACAGAACCAGGGGCCTGGGCAGTCGGAGGACACCTGCTCCGAGC
CCACCAACAAGAAGATGCGCCGCAACCGGTTTAAa

Putative encoded protein (169 amino acids), bold show WT amino acid sequence

MVSKLTSLQOELLSALLSSGVTK**EVLIQALEELL**PSNFGVK**LETLP**SPGSGADLD**TKPVFHTLTNG**
HAKGRLSGDEGSEDGDDYD**TPPI**L**KELQALNTEEA**E**QRAE**VDRMLRVQ**PSPEL**WKH**DRQKQ**SGSAA
VLSRVQ**STEP**GA**WAVGGHLLRAHQ**EDAPQ**PV***

3- SPLICED ISOFORM B Δ EXON2

cDNA sequence (underlined show spliced exon 3)

ATGGTGTCCAAGCTCACGTCGCTCCAGCAAGAACTCCTGAGTGCCCTGCTGAGCTCCGGAGTCACCAA
GGAAGTGCTGATCCAGGCCTTGGAGGAGTTACTGCCGTCCCCGAATTTTCGGGGTGAAGCTGGAGACAC
TGCCCCGTGTCCCCCGGGAGCGGGGCGGATCTCGACACCAAGCCGGTTTTCCATACTCTCACCAATGGC
CACGCCAAGGGCCGCTTGTCTGGGGACGAGGGCTCAGAGGACGGCGACGACTATGACACTCCTCCCAT
CCTCAAAGAGCTCCAGGCGCTCAACACCGAGGAGGCCGCGGAGCAGCGGGCCGAGGTGGACCGGATGC
TCAGAGTT**CAGTCAACAGAACCAGGGGCCTGGGCAGTCGGAGGACACCTGCTCCGAGCCCACCAACAA**
GAAGATGCGCCGCAACCGGTTTAAa

Putative encoded protein (143 amino acids), bold show WT amino acid sequence

MVSKLTSLQOELLSALLSSGVTK**EVLIQALEELL**PSNFGVK**LETLP**SPGSGADLD**TKPVFHTLTNG**
HAKGRLSGDEGSEDGDDYD**TPPI**L**KELQALNTEEA**E**QRAE**VDRMLRVQ**STEP**GA**WAVGGHLLRAHQ**
EDAPQ**PV***

Note that the STOP codons of putative encoded proteins are followed by a purine, which is predicted to positively influence translational termination efficiency (UAAR, UAGR, UGAR (R: purine) (McCaughan et al., 1995).

Hnf1b Mouse exon-2

CGAGGACCCGTTGGAGGGCTGCCAAAATGATCAAGGGATACATGCAACAGCACAAATATCCCCAGAGGG
AGGTGGTCGATGTCACAGGCCTGAACCAATCCCACCTCTCTCAACACCTCAACAAGGGCACCCCATG
AAGACCCAGAAGAGAGCTGCCCTGTACTCTTGTACGTCAGAAAGCAACGGGAGATCCTCCGAC

Underlined 32bp of exon 2 spliced out of mouse exon2

Western blots from embryo/adult kidneys

Human embryonic kidney (HEK) 293 cells were maintained and transiently transfected as described (Barbacci et al., 2004), with either expression vectors of full-length HNF1B or the truncated spliced isoforms (A Δ exon2: 169 amino acids; B Δ exon2: 143 amino acids, A/B Δ 32bp: 170 amino acids cloned into the pCB6 vector (Barbacci et al., 2004).

Transfected cells were washed with ice-cold PBS plus Roche protease inhibitors, scraped transferred into Eppendorf tubes and centrifuged 5 min at 3.000 rpm. The cellular pellet was resuspended into ice cold HNB buffer (0,5M Sucrose, 10 mM Tris-HCl pH 7.4, 60 mM KCl, 0,5 mM Spermidine, 0,15 mM Spermine, 1 mM DTT plus complete protease inhibitor cocktail ROCHE), freeze and thaw 4-times in liquid N₂ and centrifuged 10 min at 10.0000 rpm. The supernatant containing the whole cell extracts was frozen in liquid N₂ and kept at -80°C.

The two kidneys of each embryo of at least three (n=3) different litters were pooled, frozen in liquid N₂ and lysed in ice-cold lysis buffer using 23g and 26g syringes. Adult kidney pieces were frozen in liquid N₂, reduced to a fine powder under Liquid N₂ and further lysed in lysis buffer using a syringe. Lysis buffer contains 15% glycerol, 10 mM Tris-HCl pH 7.4, 150 mM NaCl, 5 mM EDTA, 1% NP40, 3 mM Sodium Pyrophosphate, 50 mM Sodium Fluoride with complete protease inhibitor cocktail ROCHE added before using. Samples were centrifuged for 15 minutes at 13,000 rpm 4°C, and the supernatant frozen in Liquid N₂ and kept 80°C. Protein concentration was determined using the Pierce™ BCA Protein Assay kit. Whole cell extracts containing 20-30µg of protein were prepared in SDS sample buffer and subjected to SDS-PAGE (4–15% Mini-PROTEAN® TGX™ Precast Protein Gels, Biorad). After the proteins were transferred onto a 0,2 µm nitrocellulose membrane (BioRad) and blocking with TBST (50 mM Tris-HCl pH 7.4, 150 mM NaCl, 0.1 % Tween, 5% skim milk), immunoblotting was performed by overnight incubation in TBST 1% skim milk buffer with a rabbit polyclonal antibody against HNF1B (1:500) previously validated (Haumaitre et al., 2006) raised in the laboratory against residues 39–89 of the mouse HNF1B protein as well as a Sigma HNF1B antibody (1:1000) and raised against residues 23-120 of the human HNF1B protein. Secondary horseradish peroxidase-conjugated antibodies (goat anti-rabbit; Santa Cruz Biotechnology) were incubated at room temperature in blocking buffer for 2hs. After visualization, blots were stripped and incubated with mouse monoclonal α-tubulin antibody (Sigma-Aldrich) at 1:10.000 used as a loading control and then exposed to secondary antibody as above (antibodies are listed in Table S7). Positive HNF1B bands were detected by chemiluminescence (Super Signal™ West Femto Thermo Scientific). Western lightning Plus-ECL Perkin Elmer was used to detect α-tubulin. Images were captured with G-BOX Syngene Europe, Chemoluminescence Image Capture software and quantified by Image J. *WT* and HNF1B proteins normalized by

α -tubulin expression were quantified from each litter. A *WT* sample was assigned a 100% value and the other samples of the same litter *WT* and heterozygotes were referred as a percentage of this value. This allowed the comparison of different litters of a given embryonic stage. Statistical significance was determined by using unpaired *t*-test, using GraphPad Prism 6.00 (GraphPad Software, San Diego, CA). $P < 0.05$ * was considered significant.

Plasma and urine analyses

Urine and plasma were obtained on age- and gender-matched heterozygous and *WT* mice (males). They were housed in light- and temperature-controlled room with *ad libitum* access to tap water and standard chow (Diet AO4, SAFE, France). 24-h urine samples collected under mineral oil to avoid evaporation were obtained at baseline in individual metabolic cages, after 2-3 days habituation. Each 24-h, animals were weighed and the food, water intake, urine volume and fecal weight recorded. Blood was sampled by retro-ocular puncture in general 2 weeks after being in the metabolic cages and plasma samples were kept at -80°C . The urinary concentrating ability was tested after 22h water deprivation. Urinary creatinine, urea and electrolytes, plasma urea, creatinine, magnesium, ASAT, ALAT and were measured on Olympus AU400 Chemistry Analyzer (ICB-IFR2, Laboratoire de Biochimie UFR de Médecine Paris 7, Bichat. Osmolality was measured using a vapor pressure osmometer (Wescor 5500, USA).

Statistical analysis

Data are represented as mean \pm standard error of mean (SEM). Student *t*-test or unpaired *t*-test with Welch correction when required test was used. $P < 0.05$ was considered to be significant with * $P < 0.05$, ** $P < 0.01$, *** $P < 0.001$.

Urinary proteome analysis

Urine samples were obtained from 17 *Hnf1b*^{Sp2/+} and 18 *WT* mice from 3, 8, 12, 17 month-old. Urines from *WT* and mutant mice (males) were collected by spontaneous voiding and kept frozen at -80°C or after being placed individually in metabolic cages as described. The total volume of 24-hs urines was aliquoted and frozen at -80°C . A 150 μl sample of mouse urine was diluted with the same volume of urea buffer (2 M

urea, 10 mM NH₄OH, 0.2% sodium dodecylsulfate). 150 µl of urine samples were ultrafiltered, desalted, lyophilized and resuspended for proteome analysis as described (von zur Muhlen et al., 2012).

CE-MS analysis, data processing and statistical analysis.

Capillary electrophoresis-mass coupled to spectrometry (CE-MS) analysis was performed using a Beckman Coulter Proteome Lab PA800 capillary electrophoresis system (Fullerton, CA) online coupled to a micrOTOF II MS (Bruker Daltonic, Bremen, Germany) as described (Coon et al., 2008; Mischak et al., 2013). For normalization caused by analytical variances and differences in urine dilution, MS signal intensities were normalized relative to 41 internal standard peptides generally present in at least 90% of all mouse urine samples, with small relative standard deviation (SD) (von zur Muhlen et al., 2012). The peak lists obtained characterized each peptide by its molecular mass (in Daltons), normalized CE migration time (in minutes) and normalized signal intensity. The data of all detected peptides were deposited, matched, and annotated in a Microsoft SQL database as previously described allowing further analysis and comparison of multiple samples (Siwy et al., 2011). The main differences of peptides between the *WT* and *Hnf1b*^{Sp2/+} urines were obtained using the P-values based on Wilcoxon rank-sum test. **Statistical adjustment of P-values** due to multiple testing, was performed by the Benjamini and Hochberg method. Peptides that were detectable in >90% of mice and reached an adjusted P-value of <0.05 were further considered as relevant.

Transcriptional profiling at different stages by mRNA-sequencing

The two kidneys from heterozygous *Hnf1b*^{Sp2/+} mutants and *WT* embryos in the C57BL/6N background were microdissected from the same litter. This requirement limited the number of samples used in general to 2 *WT*s and 2 heterozygous mutants, independently of the sex. Note that we found a similar phenotype in males and females. The stages analyzed included E14.5 (when morphologically the mutant kidneys were morphological normal and considered as pre-disease and at disease stages E15.5, E17.5 and postnatal day 1 (P1). Note that at E15.5 we performed deep sequencing from pooled samples of 3 *WT* and 3 *Hnf1b*^{Sp2/+} (6 kidneys each sample). RNA seq; from E14.5, 15.5 and P1 was performed at Alexander Fleming Institute, Genomics Facility, Greece, while E17.5 at FASTERIS.

Stade	WT	WT	<i>Hnf1b</i> ^{Sp2/+}	<i>Hnf1b</i> ^{Sp2/+}
E14.5	SCR10-E145-4wt	SCR13-E144wt	SCR12-E145 HET	SCR15-E145-HET
E15.5	WT (Pool n=3)		TR (Pool n=3)	
E17.5 *	GZS 17	GZS 35 (n=3)	GSZ 34 (n=3)	GSZ 36 (n=3)
P1	SCR20_P1_	SCR21_P1_	SCR22 P1	SCR23_P1

*RNA was prepared from the 2 kidneys of each embryo, except when the n is indicated (i.e. E15.5 and E17.5) * RNA from 2 litters born the same day in the same cage (Pool n=3, 6 kidneys)*

RNA from microdissected kidneys was extracted by Tryzol, using the miRNA mini kit Qiagen for the extraction of total and miRNAs. The quality of the RNA samples was assessed on the Agilent Bioanalyzer system using the Agilent RNA 6000 Nano Kit (Agilent Technologies) and RNA with a RIN higher than 8 was used. 1-2 µg of total RNA were used for mRNA isolation using the Dynabeads® mRNA DIRECT™ Micro Kit (ThermoFisher Scientific). mRNA was digested with RNase III, purified, hybridized and ligated to Ion Adaptors, reverse transcribed, barcoded and amplified, using the Ion Total RNA-Seq Kit v2 (ThermoFisher Scientific). RNA sequencing was performed on an Ion Proton™ System, according to the manufacturer's instructions. The prepared libraries were quantified and pooled together in duplicates at the required concentration. The pools were then processed on an OneTouch 2 instrument and enriched on a One Touch ES station. Templating was performed using the Ion PI™ Template OT2 200 Kit (ThermoFisher Scientific) and sequencing with the Ion PI™ Sequencing 200 Kit on Ion Proton PI™ chips (ThermoFisher Scientific) according to commercial protocols. The resulting RNA-Seq BAM files were analyzed with the Bioconductor package metaseqR (Moulos and Hatzis, 2015) and applying the edgeR methodology for differential expression analysis with default settings (<http://www.bioconductor.org/packages/release/bioc/html/edgeR.html>).

RNA-sequencing from E17.5 embryo kidneys was performed by FASTERIS-Genome Analyzer Service (Switzerland). High-throughput DNA sequencing using Illumina technology consisted of processing in vitro samples to generate a library of short inserts (the DNA Colonies Template Library). The library was sequenced on the

Illumina HiSeq 2000. For each lane 130-150 million DNA colonies producing pass filter sequences were assured. The read lengths are 1x50 or 1x100 base pairs (bp) for single-reads runs using the forward sequencing primer. The inserts can also be sequenced from both ends using a 'forward' and a 'reverse' sequencing primer, generating pairedreads of 2x100 bp. The data were processed using bioinformatics tools to extract biologically useful information. To homogenize mRNA-seq comparisons, RNA-seq files were all analyzed as described above (Moulos and Hatzis, 2015).

ACKNOWLEDGMENTS

We thank Gunjan Pandey (Medical University Heidelberg) for critical reading of the manuscript. We also thank the ICS for the generation of the mouse model, providing ES heterozygous mutant clones and useful discussions, Sophie Gournet for illustrations, Mélanie Fabre for help in the initial analysis, Edouard Manzoni for animal care, Pantelis Hatzis (Alexander Fleming Institute, Genomics Facility, Greece) for mRNA sequencing, Christophe Antoniewsky (IBPS UMR7622) for help in mRNA-seq statistical analyses, Mark Knepper (Bethesda USA), Renata Kozyraki (Institut Cordeliers, France), Sylvie Robine (Institut Curie, Paris) and Matias DeVas and Jorge Ferrer (Imperial College London) for kindly providing antibodies.

FUNDINGS

L.N and M. K were early researchers (ER) supported by the by the Biology of Liver and Pancreatic Development and Disease (BOLD) Marie Curie Initial Training Network (MCITN) EU-FP7 programme (No. 238821); P. R. and P.M. were recipients of PhD student fellowships from ITN RENALTRACT MSCA-ITN-2014-642937. C. L. was a postdoctoral researcher supported by Agence National de la Recherche (ANR) Blan06-2_139420.

This work was supported by the GIS-Institut Maladies Rares Paris France & Institut Clinique de la Souris, Ilkirch, France, the Agence National de la Recherche (ANR) Blan06-2_139420; the Institut National de la Santé et de la Recherche Médicale (INSERM, France); the BOLD Marie Curie Initial Training Network (MCITN) EU-FP7 programme (No. 238821); by the European Union's Horizon 2020 Research and Innovation Programme under the Marie Skłodowska-Curie grant agreement No. 642937 (RENALTRACT; MSCA-ITN-2014-642937); the Centre National de la Recherche Scientifique (CNRS) and the Sorbonne Université (TO S.C.).

M.U. was supported by CNRS, Sorbonne Université and RENALTRACT MSCA-ITN-2014-642937. P.M. and P.R. by RENALTRACT MSCA-ITN-2014-642937

DATA AVAILABILITY: RNA-Seq data sets are accessible through GEO: **GSE159566**

COMPETING INTERESTS STATEMENT: The authors declare no competing interests.

REFERENCES

- Aboudehen, K., Nouredine, L., Cobo-Stark, P., Avdulov, S., Farahani, S., Gearhart, M. D., Bichet, D. G., Pontoglio, M., Patel, V. and Igarashi, P. (2017). Hepatocyte Nuclear Factor-1beta Regulates Urinary Concentration and Response to Hypertonicity. *J Am Soc Nephrol* 28, 2887-2900.
- Adalat, S., Hayes, W. N., Bryant, W. A., Booth, J., Woolf, A. S., Kleta, R., Subtil, S., Clissold, R., Colclough, K., Ellard, S. et al. (2019). HNF1B Mutations Are Associated With a Gitelman-like Tubulopathy That Develops During Childhood. *Kidney Int Rep* 4, 1304-11.
- Adalat, S., Woolf, A. S., Johnstone, K. A., Wirsing, A., Harries, L. W., Long, D. A., Hennekam, R. C., Ledermann, S. E., Rees, L., van't Hoff, W. et al. (2009). HNF1B mutations associate with hypomagnesemia and renal magnesium wasting. *J Am Soc Nephrol* 20, 1123-31.
- Alvelos, M. I., Rodrigues, M., Lobo, L., Medeira, A., Sousa, A. B., Simao, C. and Lemos, M. C. (2015). A novel mutation of the HNF1B gene associated with hypoplastic glomerulocystic kidney disease and neonatal renal failure: a case report and mutation update. *Medicine (Baltimore)* 94, e469.
- Bar-Even, A., Paulsson, J., Maheshri, N., Carmi, M., O'Shea, E., Pilpel, Y. and Barkai, N. (2006). Noise in protein expression scales with natural protein abundance. *Nat Genet* 38, 636-43.
- Barbacci, E., Chalkiadaki, A., Masdeu, C., Haumaitre, C., Lokmane, L., Loirat, C., Cloarec, S., Talianidis, I., Bellanne-Chantelot, C. and Cereghini, S. (2004). HNF1beta/TCF2 mutations impair transactivation potential through altered co-regulator recruitment. *Hum Mol Genet* 13, 3139-49.
- Barbacci, E., Reber, M., Ott, M. O., Breillat, C., Huetz, F. and Cereghini, S. (1999). Variant hepatocyte nuclear factor 1 is required for visceral endoderm specification. *Development* 126, 4795-805.
- Barefield, D., Kumar, M., Gorham, J., Seidman, J. G., Seidman, C. E., de Tombe, P. P. and Sadayappan, S. (2015). Haploinsufficiency of MYBPC3 exacerbates the development of hypertrophic cardiomyopathy in heterozygous mice. *J Mol Cell Cardiol* 79, 234-43.
- Bellanne-Chantelot, C., Chauveau, D., Gautier, J. F., Dubois-Laforgue, D., Clauin, S., Beaufile, S., Wilhelm, J. M., Boitard, C., Noel, L. H., Velho, G. et al. (2004). Clinical spectrum associated with hepatocyte nuclear factor-1beta mutations. *Ann Intern Med* 140, 510-7.
- Bellanne-Chantelot, C., Clauin, S., Chauveau, D., Collin, P., Daumont, M., Douillard, C., Dubois-Laforgue, D., Dusselier, L., Gautier, J. F., Jadoul, M. et al. (2005). Large genomic rearrangements in the hepatocyte nuclear factor-1beta (TCF2) gene are the most frequent cause of maturity-onset diabetes of the young type 5. *Diabetes* 54, 3126-32.
- Bingham, C., Bulman, M. P., Ellard, S., Allen, L. I., Lipkin, G. W., Hoff, W. G., Woolf, A. S., Rizzoni, G., Novelli, G., Nicholls, A. J. et al. (2001). Mutations in the hepatocyte nuclear factor-1beta gene are associated with familial hypoplastic glomerulocystic kidney disease. *Am J Hum Genet* 68, 219-24.
- Bingham, C., Ellard, S., van't Hoff, W. G., Simmonds, H. A., Marinaki, A. M., Badman, M. K., Winocour, P. H., Stride, A., Lockwood, C. R., Nicholls, A. J. et al. (2003). Atypical familial juvenile hyperuricemic nephropathy associated with a hepatocyte nuclear factor-1beta gene mutation. *Kidney Int* 63, 1645-51.

Boj, S. F., Petrov, D. and Ferrer, J. (2010). Epistasis of transcriptomes reveals synergism between transcriptional activators Hnf1alpha and Hnf4alpha. *PLoS Genet* 6, e1000970.

Bonzo, J. A., Patterson, A. D., Krausz, K. W. and Gonzalez, F. J. (2010). Metabolomics identifies novel Hnf1alpha-dependent physiological pathways in vivo. *Mol Endocrinol* 24, 2343-55.

Casemayou, A., Fournel, A., Bagattin, A., Schanstra, J., Belliere, J., Decramer, S., Marsal, D., Gillet, M., Chassaing, N., Huart, A. et al. (2017). Hepatocyte Nuclear Factor-1beta Controls Mitochondrial Respiration in Renal Tubular Cells. *J Am Soc Nephrol* 28, 3205-17.

Chen, J., Bardes, E. E., Aronow, B. J. and Jegga, A. G. (2009). ToppGene Suite for gene list enrichment analysis and candidate gene prioritization. *Nucleic Acids Res* 37, W305-11.

Chen, Y. Z., Gao, Q., Zhao, X. Z., Chen, Y. Z., Bennett, C. L., Xiong, X. S., Mei, C. L., Shi, Y. Q. and Chen, X. M. (2010). Systematic review of TCF2 anomalies in renal cysts and diabetes syndrome/maturity onset diabetes of the young type 5. *Chin Med J (Engl)* 123, 3326-33.

Chen, Z., Migeon, T., Verpont, M. C., Zaidan, M., Sado, Y., Kerjaschki, D., Ronco, P. and Plaisier, E. (2016). HANAC Syndrome Col4a1 Mutation Causes Neonate Glomerular Hyperpermeability and Adult Glomerulocystic Kidney Disease. *J Am Soc Nephrol* 27, 1042-54.

Clissold, R. L., Hamilton, A. J., Hattersley, A. T., Ellard, S. and Bingham, C. (2015). HNF1B-associated renal and extra-renal disease-an expanding clinical spectrum. *Nat Rev Nephrol* 11, 102-12.

Coffinier, C., Barra, J., Babinet, C. and Yaniv, M. (1999). Expression of the vHNF1/HNF1beta homeoprotein gene during mouse organogenesis. *Mech Dev* 89, 211-3.

Coffinier, C., Gresh, L., Fiette, L., Tronche, F., Schutz, G., Babinet, C., Pontoglio, M., Yaniv, M. and Barra, J. (2002). Bile system morphogenesis defects and liver dysfunction upon targeted deletion of HNF1beta. *Development* 129, 1829-38.

Coon, J. J., Zurbig, P., Dakna, M., Dominiczak, A. F., Decramer, S., Fliser, D., Frommberger, M., Golovko, I., Good, D. M., Herget-Rosenthal, S. et al. (2008). CE-MS analysis of the human urinary proteome for biomarker discovery and disease diagnostics. *Proteomics Clin Appl* 2, 964.

David-Silva, A., Freitas, H. S., Okamoto, M. M., Sabino-Silva, R., Schaan, B. D. and Machado, U. F. (2013). Hepatocyte nuclear factors 1alpha/4alpha and forkhead box A2 regulate the solute carrier 2A2 (Slc2a2) gene expression in the liver and kidney of diabetic rats. *Life Sci* 93, 805-13.

De Vas, M. G., Kopp, J. L., Heliot, C., Sander, M., Cereghini, S. and Haumaitre, C. (2015). Hnf1b controls pancreas morphogenesis and the generation of Ngn3+ endocrine progenitors. *Development* 142, 871-82.

Desgrange, A., Heliot, C., Skovorodkin, I., Akram, S. U., Heikkila, J., Ronkainen, V. P., Miinalainen, I., Vainio, S. J. and Cereghini, S. (2017). HNF1B controls epithelial organization and cell polarity during ureteric bud branching and collecting duct morphogenesis. *Development* 144, 4704-19.

Devuyst, O., Olinger, E., Weber, S., Eckardt, K. U., Knoch, S., Rampoldi, L. and Bleyer, A. J. (2019). Autosomal dominant tubulointerstitial kidney disease. *Nat Rev Dis Primers* 5, 60.

Edghill, E. L., Bingham, C., Ellard, S. and Hattersley, A. T. (2006). Mutations in hepatocyte nuclear factor-1beta and their related phenotypes. *J Med Genet* 43, 84-90.

Faguer, S., Decramer, S., Devuyst, O., Lengele, J. P., Fournie, G. J. and Chauveau, D. (2012). Expression of renal cystic genes in patients with HNF1B mutations. *Nephron Clin Pract* 120, c71-8.

Ferre, S. and Igarashi, P. (2018). New insights into the role of HNF-1beta in kidney (patho)physiology. *Pediatr Nephrol.* 34(8):1325-35.

Fiorentino, A., Christophorou, A., Massa, F., Garbay, S., Chiral, M., Ramsing, M., Rasmussen, M., Gubler, M., Bessieres, B., Heidet, L. et al. (2020). Developmental Renal Glomerular Defects at the Origin of Glomerulocystic Disease *Cell Rep* 33, 108304.

Gresh, L., Fischer, E., Reimann, A., Tanguy, M., Garbay, S., Shao, X., Hiesberger, T., Fiette, L., Igarashi, P., Yaniv, M. et al. (2004). A transcriptional network in polycystic kidney disease. *EMBO J* 23, 1657-68.

Haldorsen, I. S., Vesterhus, M., Raeder, H., Jensen, D. K., Sovik, O., Molven, A. and Njolstad, P. R. (2008). Lack of pancreatic body and tail in HNF1B mutation carriers. *Diabet Med* 25, 782-7.

Harries, L. W., Bingham, C., Bellanne-Chantelot, C., Hattersley, A. T. and Ellard, S. (2005). The position of premature termination codons in the hepatocyte nuclear factor - 1 beta gene determines susceptibility to nonsense-mediated decay. *Hum Genet* 118, 214-24.

Harries, L. W., Ellard, S., Jones, R. W., Hattersley, A. T. and Bingham, C. (2004). Abnormal splicing of hepatocyte nuclear factor-1 beta in the renal cysts and diabetes syndrome. *Diabetologia* 47, 937-42.

Haumaitre, C., Barbacci, E., Jenny, M., Ott, M. O., Gradwohl, G. and Cereghini, S. (2005). Lack of TCF2/vHNF1 in mice leads to pancreas agenesis. *Proc Natl Acad Sci U S A* 102, 1490-5.

Haumaitre, C., Fabre, M., Cormier, S., Baumann, C., Delezoide, A. L. and Cereghini, S. (2006). Severe pancreas hypoplasia and multicystic renal dysplasia in two human fetuses carrying novel HNF1beta/MODY5 mutations. *Hum Mol Genet* 15, 2363-75.

Heidet, L., Decramer, S., Pawtowski, A., Moriniere, V., Bandin, F., Knebelmann, B., Lebre, A. S., Faguer, S., Guignon, V., Antignac, C. et al. (2010). Spectrum of HNF1B mutations in a large cohort of patients who harbor renal diseases. *Clin J Am Soc Nephrol* 5, 1079-90.

Heliot, C., Desgrange, A., Buisson, I., Prunskaitė-Hyyryläinen, R., Shan, J., Vainio, S., Umbhauer, M. and Cereghini, S. (2013). HNF1B controls proximal-intermediate nephron segment identity in vertebrates by regulating Notch signalling components and *Irx1/2*. *Development* 140, 873-85.

Hiesberger, T., Shao, X., Gourley, E., Reimann, A., Pontoglio, M. and Igarashi, P. (2005). Role of the hepatocyte nuclear factor-1beta (HNF-1beta) C-terminal domain in *Pkhd1* (ARPKD) gene transcription and renal cystogenesis. *J Biol Chem* 280, 10578-86.

Hopp, K., Ward, C. J., Hommerding, C. J., Nasr, S. H., Tuan, H. F., Gainullin, V. G., Rossetti, S., Torres, V. E. and Harris, P. C. (2012). Functional polycystin-1 dosage governs autosomal dominant polycystic kidney disease severity. *J Clin Invest.* 122, 4257-73.

Iwasaki, N., Ogata, M., Tomonaga, O., Kuroki, H., Kasahara, T., Yano, N. and Iwamoto, Y. (1998). Liver and kidney function in Japanese patients with maturity-onset diabetes of the young. *Diabetes Care* 21, 2144-8.

Johnson, A., Nguyen, H. T. and Veitia, R. (2019). Causes and effects of haploinsufficiency. *Biol Rev Camb Philos Soc* 94, 1774-85.

Kettunen, J. L. T., Parviainen, H., Miettinen, P. J., Farkkila, M., Tamminen, M., Salonen, P., Lantto, E. and Tuomi, T. (2017). Biliary Anomalies in Patients With HNF1B Diabetes. *J Clin Endocrinol Metab* 102, 2075-82.

Kikuchi, R., Kusuhara, H., Hattori, N., Kim, I., Shiota, K., Gonzalez, F. J. and Sugiyama, Y. (2007). Regulation of tissue-specific expression of the human and mouse urate transporter 1 gene by hepatocyte nuclear factor 1 alpha/beta and DNA methylation. *Mol Pharmacol* 72, 1619-25.

Kornfeld, J. W., Baitzel, C., Konner, A. C., Nicholls, H. T., Vogt, M. C., Herrmanns, K., Scheja, L., Haumaitre, C., Wolf, A. M., Knippschild, U. et al. (2013). Obesity-induced overexpression of miR-802 impairs glucose metabolism through silencing of Hnf1b. *Nature* 494, 111-5.

Kyrmizi, I., Hatzis, P., Katrakili, N., Tronche, F., Gonzalez, F. J. and Talianidis, I. (2006). Plasticity and expanding complexity of the hepatic transcription factor network during liver development. *Genes Dev* 20, 2293-305.

Lee, Y. H., Sauer, B. and Gonzalez, F. J. (1998). Laron dwarfism and non-insulin-dependent diabetes mellitus in the Hnf-1alpha knockout mouse. *Mol Cell Biol* 18, 3059-68.

Lennerz, J. K., Spence, D. C., Iskandar, S. S., Dehner, L. P. and Liapis, H. (2010). Glomerulocystic kidney: one hundred-year perspective. *Arch Pathol Lab Med* 134, 583-605.

Lindner, T. H., Njolstad, P. R., Horikawa, Y., Bostad, L., Bell, G. I. and Sovik, O. (1999). A novel syndrome of diabetes mellitus, renal dysfunction and genital malformation associated with a partial deletion of the pseudo-POU domain of hepatocyte nuclear factor-1beta. *Hum Mol Genet* 8, 2001-8.

Lokmane, L., Haumaitre, C., Garcia-Villalba, P., Anselme, I., Schneider-Maunoury, S. and Cereghini, S. (2008). Crucial role of vHNF1 in vertebrate hepatic specification. *Development* 135, 2777-86.

Lokmane, L., Heliot, C., Garcia-Villalba, P., Fabre, M. and Cereghini, S. (2010). vHNF1 functions in distinct regulatory circuits to control ureteric bud branching and early nephrogenesis. *Development* 137, 347-57.

Marable, S. S., Chung, E. and Park, J. S. (2020). Hnf4a Is Required for the Development of Cdh6-Expressing Progenitors into Proximal Tubules in the Mouse Kidney. *J Am Soc Nephrol*, DOI : 10.1681/ASN.2020020184.

Martovetsky, G., Tee, J. B. and Nigam, S. K. (2013). Hepatocyte nuclear factors 4alpha and 1alpha regulate kidney developmental expression of drug-metabolizing enzymes and drug transporters. *Mol Pharmacol* 84, 808-23.

Massa, F., Garbay, S., Bouvier, R., Sugitani, Y., Noda, T., Gubler, M. C., Heidet, L., Pontoglio, M. and Fischer, E. (2013). Hepatocyte nuclear factor 1beta controls nephron tubular development. *Development* 140, 886-96.

Mattapallil, M. J., Wawrousek, E. F., Chan, C. C., Zhao, H., Roychoudhury, J., Ferguson, T. A. and Caspi, R. R. (2012). The Rd8 mutation of the Crb1 gene is present in vendor lines of C57BL/6N mice and embryonic stem cells, and confounds ocular induced mutant phenotypes. *Invest Ophthalmol Vis Sci* 53, 2921-7.

McCaughan, K. K., Brown, C. M., Dalphin, M. E., Berry, M. J. and Tate, W. P. (1995). Translational termination efficiency in mammals is influenced by the base following the stop codon. *Proc Natl Acad Sci USA* 92, 5431-35.

Michael, L., Sweeney, D. E. and Davies, J. A. (2007). The lectin Dolichos biflorus agglutinin is a sensitive indicator of branching morphogenetic activity in the developing mouse metanephric collecting duct system. *J. Anat.* 210, 89-97.

Mischak, H., Vlahou, A. and Ioannidis, J. P. (2013). Technical aspects and inter-laboratory variability in native peptide profiling: the CE-MS experience. *Clin Biochem* 46, 432-43.

Moulos, P. and Hatzis, P. (2015). Systematic integration of RNA-Seq statistical algorithms for accurate detection of differential gene expression patterns. *Nucleic Acids Res* 43, e25.

Nakayama, M., Nozu, K., Goto, Y., Kamei, K., Ito, S., Sato, H., Emi, M., Nakanishi, K., Tsuchiya, S. and Iijima, K. (2010). HNF1B alterations associated with congenital anomalies of the kidney and urinary tract. *Pediatr Nephrol* 25, 1073-9.

Paces-Fessy, M., Fabre, M., Lesaulnier, C. and Cereghini, S. (2012). Hnf1b and Pax2 cooperate to control different pathways in kidney and ureter morphogenesis. *Hum Mol Genet* 21, 3143-55.

Quilichini, E., Fabre, M., Nord, C., Dirami, T., Le Marec, A., Cereghini, S., Pasek, R.C., Gannon, M., Ahlgren, U. and Haumaitre, C. Insights into the etiology and physiopathology of MODY5/HNF1B pancreatic phenotype with a mouse model of the human disease. *The Journal of Pathology*, in press.

Ricci, P., Magalhaes, P., Krochmal, M., Pejchinovski, M., Daina, E., Caruso, M. R., Goea, L., Belczacka, I., Remuzzi, G., Umbhauer, M. et al. (2019). Urinary proteome signature of Renal Cysts and Diabetes syndrome in children. *Sci Rep* 9, 2225.

Rio Frio, T., Wade, N. M., Ransijn, A., Berson, E. L., Beckmann, J. S. and Rivolta, C. (2008). Premature termination codons in PRPF31 cause retinitis pigmentosa via haploinsufficiency due to nonsense-mediated mRNA decay. *J Clin Invest*. 118(4):1519-31.

Rousseau, A. and Bertolotti, A. (2018). Regulation of proteasome assembly and activity in health and disease. *Nat Rev Mol Cell Biol*. 19(11):697-712.

Saji, T., Kikuchi, R., Kusuhara, H., Kim, I., Gonzalez, F. J. and Sugiyama, Y. (2008). Transcriptional regulation of human and mouse organic anion transporter 1 by hepatocyte nuclear factor 1 alpha/beta. *J Pharmacol Exp Ther* 324, 784-90.

Shao, A., Chan, S. C. and Igarashi, P. (2020). Role of transcription factor hepatocyte nuclear factor-1beta in polycystic kidney disease. *Cell Signal* 71, 109568.

Siwy, J., Mullen, W., Golovko, I., Franke, J. and Zurbig, P. (2011). Human urinary peptide database for multiple disease biomarker discovery. *Proteomics Clin Appl* 5, 367-74.

Terryn, S., Tanaka, K., Lengele, J. P., Olinger, E., Dubois-Laforgue, D., Garbay, S., Kozyraki, R., Van Der Smissen, P., Christensen, E. I., Courtoy, P. J. et al. (2016). Tubular proteinuria in patients with HNF1alpha mutations: HNF1alpha drives endocytosis in the proximal tubule. *Kidney Int* 89, 1075-89.

Thiagarajan, R. D., Georgas, K. M., Rumballe, B. A., Lesieur, E., Chiu, H. S., Taylor, D., Tang, D. T., Grimmond, S. M. and Little, M. H. (2011). Identification of anchor genes during kidney development defines ontological relationships, molecular subcompartments and regulatory pathways. *PLoS One* 6, e17286.

Torell, F., Bennett, K., Cereghini, S., Fabre, M., Rannar, S., Lundstedt-Enkel, K., Moritz, T., Haumaitre, C., Trygg, J. and Lundstedt, T. (2018). Metabolic profiling of multi-organ samples - Evaluation of MODY5/RCAD mutant mice. *J Proteome Res*. 17(7):2293-2306.

von zur Muhlen, C., Schiffer, E., Sackmann, C., Zurbig, P., Neudorfer, I., Zirlik, A., Htun, N., Iphofer, A., Jansch, L., Mischak, H. et al. (2012). Urine proteome analysis reflects atherosclerotic disease in an ApoE-/- mouse model and allows the discovery of new

candidate biomarkers in mouse and human atherosclerosis. *Mol Cell Proteomics* 11, M111 013847.

Wilson, P. D. (2011). Apico-basal polarity in polycystic kidney disease epithelia. *Biochim Biophys Acta* 1812, 1239-48.

You, K. T., Li, L. S., Kim, N. G., Kang, H. J., Koh, K. H., Chwae, Y. J., Kim, K. M., Kim, Y. K., Park, S. M., Jang, S. K. et al. (2007). Selective translational repression of truncated proteins from frameshift mutation-derived mRNAs in tumors. *PLoS Biol* 5, e109.

Yu, D. D., Guo, S. W., Jing, Y. Y., Dong, Y. L. and Wei, L. X. (2015). A review on hepatocyte nuclear factor-1beta and tumor. *Cell Biosci* 13, 5-58.

Figures

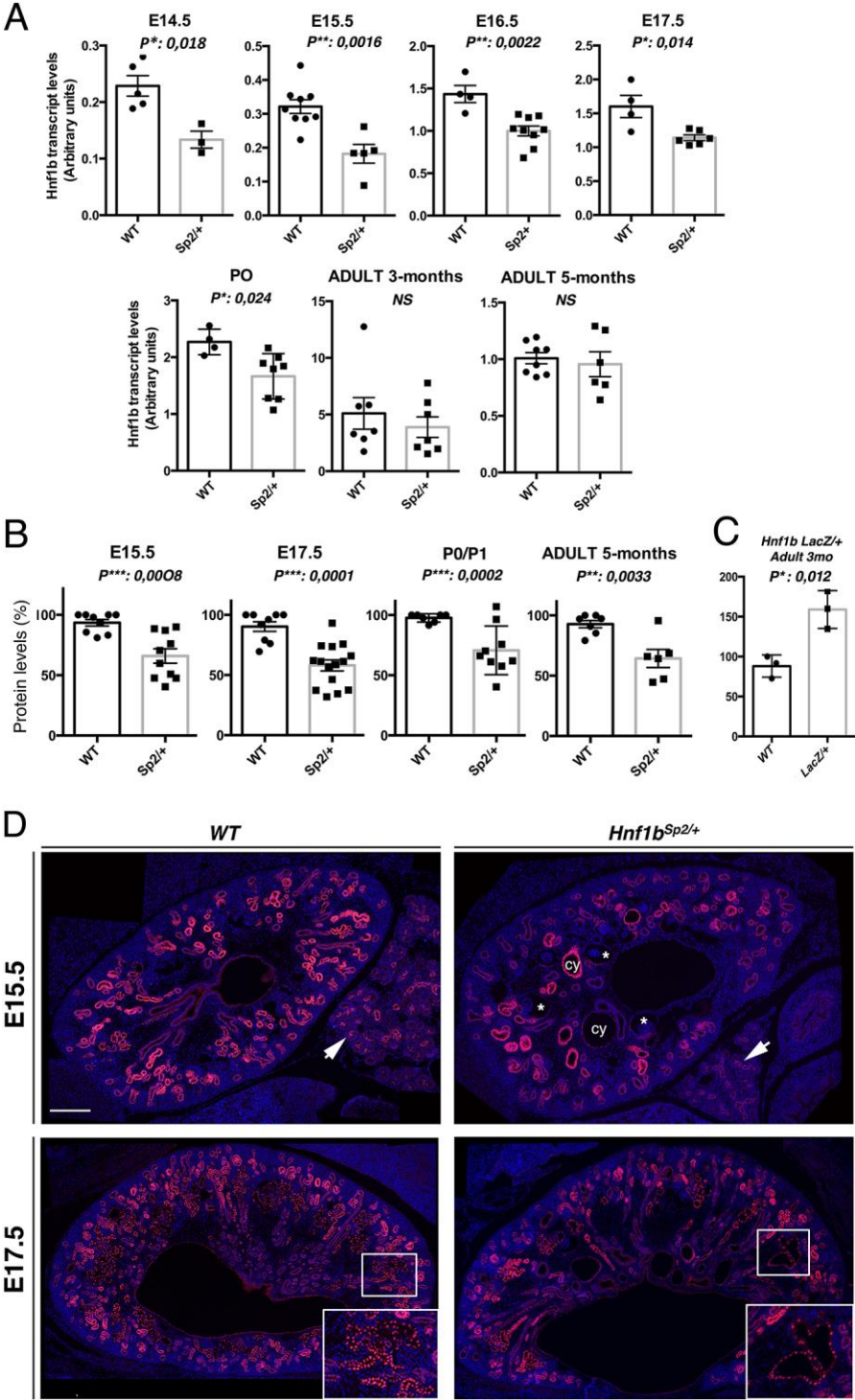


Figure 1: Expression levels of normal *Hnf1b* transcripts and protein from *WT* and *Hnf1b*^{Sp2/+} heterozygous mutants

(A) qRT-PCR of normal *Hnf1b* transcripts in *WT* and *Hnf1b*^{Sp2/+} kidneys at the indicated stages. *WT* versus *Hnf1b*^{Sp2/+} sample numbers were: E14.5= 5 vs 3; E15.5= 9 vs 5; E16.5= 4 vs 9; E17.5= 4 vs 6; at P0= 4 vs 8; adults 3-months =7 vs 7 and adults 5-months= 8 vs 6. Significant decreases in *Hnf1b* transcript relative to *WT* were at E14.5= 58,5%, E15.5=57%, E16.5=50%, P0=64%. **(B)** Western blot quantification of HNF1B protein levels in *Hnf1b*^{Sp2/+} relative to *WT*. Significant decreases to 70%; 62%; 72% and 69% relative to *WT* were observed respectively at E15.5, E17.5, P0 and adults 5-months. **(C)** Western-blot quantification of 3-months-old *WT* and heterozygous *Hnf1b*^{LacZ/+} show an increase of 98% in HNF1B levels. Error bars represent standard error of the mean (SEM). Unpaired *t*-test, $p < 0,05$ (*), $p < 0,01$ (**); $p < 0,001$ (***). **(D)** HNF1B immunostaining of E15.5 and E17.5 embryo sections show in *Hnf1b*^{Sp2/+} kidneys a global decrease in the number of HNF1B+ structures together with decreased nuclear staining in some regions (magnification in E17.5). Note adjacent pancreatic ducts exhibiting also decreased HNF1B expression Glomerular cysts (cy) and nuclear staining in both non-dilated and dilated renal tubules (*). E15.5 cysts HNF1B+: a PT and a weaker labeled cyst (potentially glomerular). Scale bar: 200 μ m

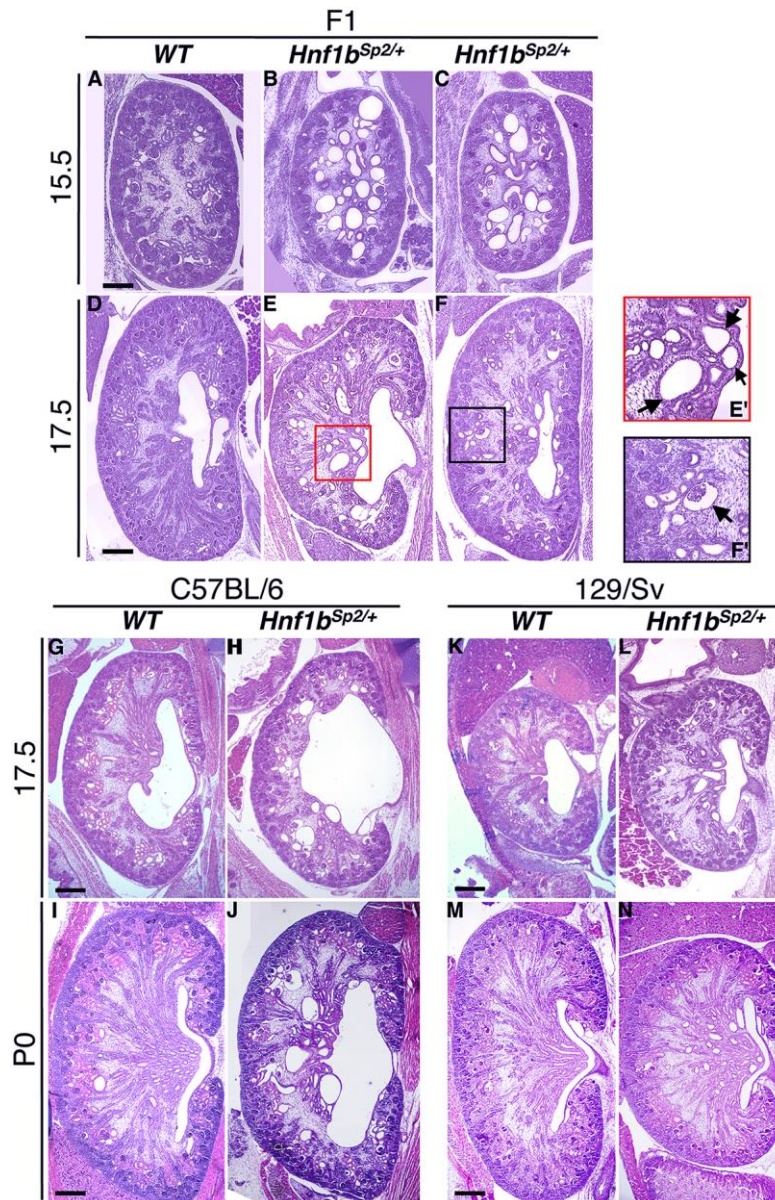


Figure 2: Histology of *Hnf1b*^{Sp2/+} embryos from different genetic backgrounds highlights the early onset of renal cysts and hydronephrosis

(A-F) Representative Hematoxylin and Eosin (H&E) staining sections of embryo kidneys show glomerular cysts and tubular dilatations in the medulla at E15.5 and E17.5 (arrows in E', higher magnification of E). F' (higher magnification of F): arrow show cystic glomeruli. Embryos were from a mixed background (F1).

(G-N) Inbred onto C57BL/6N and 129/sv backgrounds show different phenotype severity. Note in C57BL/6N background pelvic dilatations at E17.5 (H), hydronephrosis and duplicated kidney at P0 (H, J) (See also Fig.S4), in addition to cystic glomeruli and medullar tubules dilatations (H, J) also observed in 129/sv background (L, N). Images are representative of $n = 6$ for each genotype. Scale bar: 200 μ m.

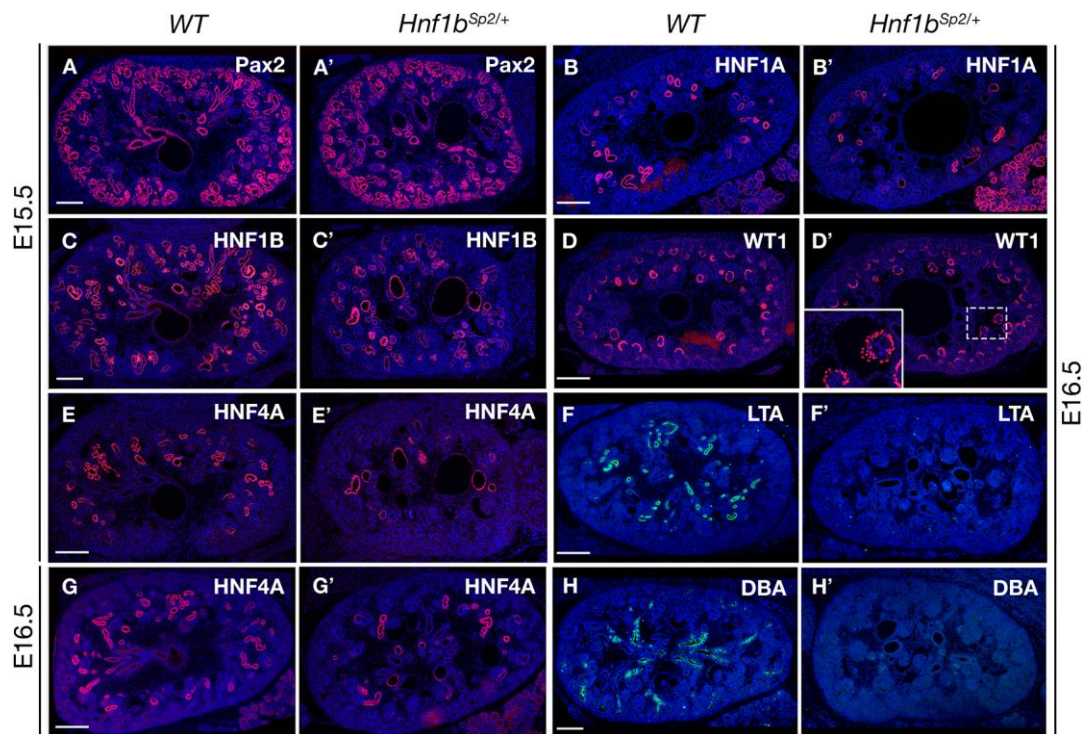


Figure 3: *Hnf1b*^{Sp2/+} exhibit normal ureteric bud branching but glomerular cysts and delayed proximal tubule differentiation. Immunohistochemical analysis of *WT* and *Hnf1b*^{Sp2/+} embryo kidneys with PAX2 (A, A'), HNF1B (C, C'), the PT markers HNF4A (E, E', G, G'), HNF1A (B, B'), and LTA (F, F'), WT1 (D, D', inset glomerular cyst magnification with partially disorganized podocyte expression), and the collecting duct lectin DBA (F, F') at indicated stages. Note in *Hnf1b*^{Sp2/+} sections decreased HNF4A+ PT-structures (E', G') and PT dilatations particularly at E15.5 (E'), which correlate with HNF1B expression in a serial section (C') of the same embryo, decreased HNF1A PT expression together with increased acinar pancreatic expression (G') and the absence of lectins LTA (D') and DBA (F'). Sections are co-stained with DAPI. Scale bar: 200µm.

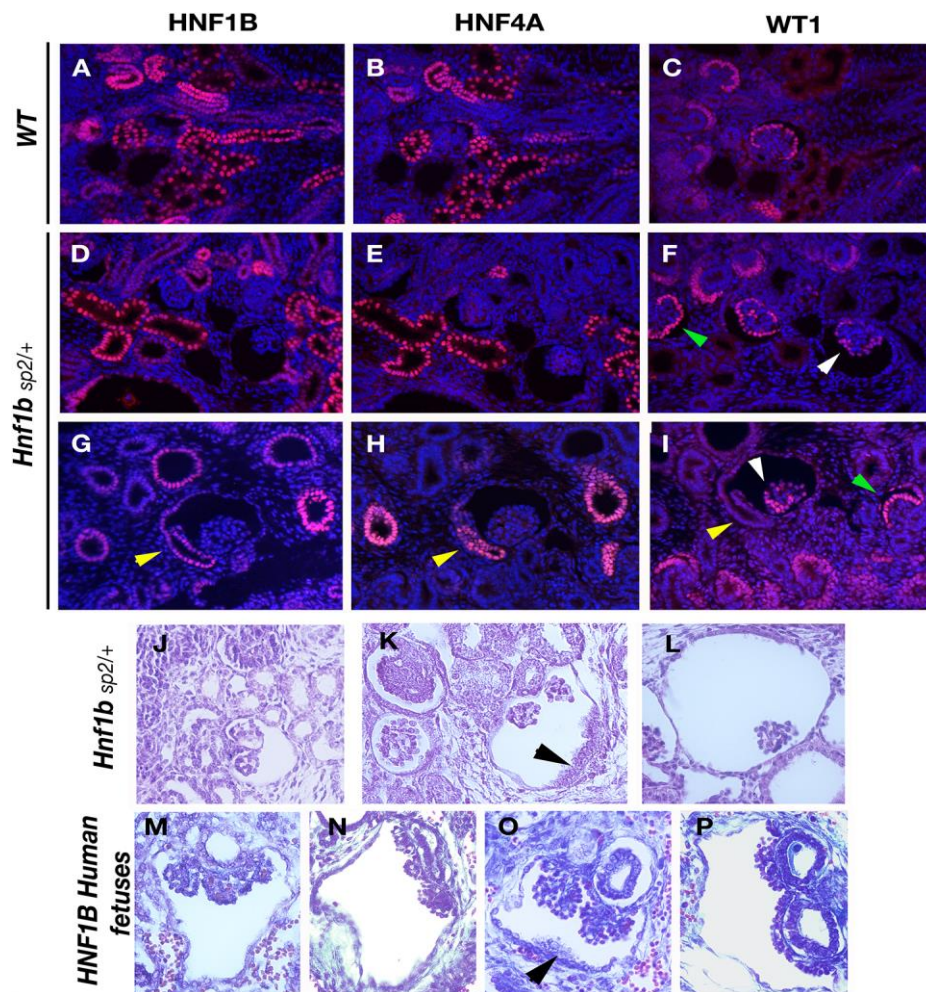


Figure 4: Glomerular cyst development, progressive tuft atrophy and abnormal PT implantation in *Hnf1b*^{Sp2/+} embryos. Histological comparison with human *HNF1B* mutant fetuses.

Immunohistochemical analysis of E16.5 *WT* (A-C) and *Hnf1b*^{Sp2/+} embryos (D-I). PTs are highlighted by the co-expression of HNF4A and HNF1B, while developing glomeruli and condensed mesenchyme by WT1 staining. Sections are co-stained with DAPI. Note that HNF4A staining in *Hnf1b*^{Sp2/+} (E, H) was intentionally increased to better visualize positive PTs. Note in *Hnf1b*^{Sp2/+} dilated PTs HNF4A+ (E, H), glomerular cysts with disorganized podocyte layer stained by WT1 (white arrows F, I), while non-cystic glomeruli show normal podocyte layer (green arrows). Yellow arrows (H-I) show abnormal lateral insertion of the glomerulotubular junction into Bowman's capsule and disorganized HNF4A expression (H). H&E-staining of E17.5 *Hnf1b*^{Sp2/+} embryos (J-L) and human mutant fetuses described in (Haumaitre et al., 2006) (M-P). Black arrows: disorganized layer cells in mutants and human fetuses (K, O). Note also collapsed or disrupted tufts inside highly widened Bowman's capsules (L, P).

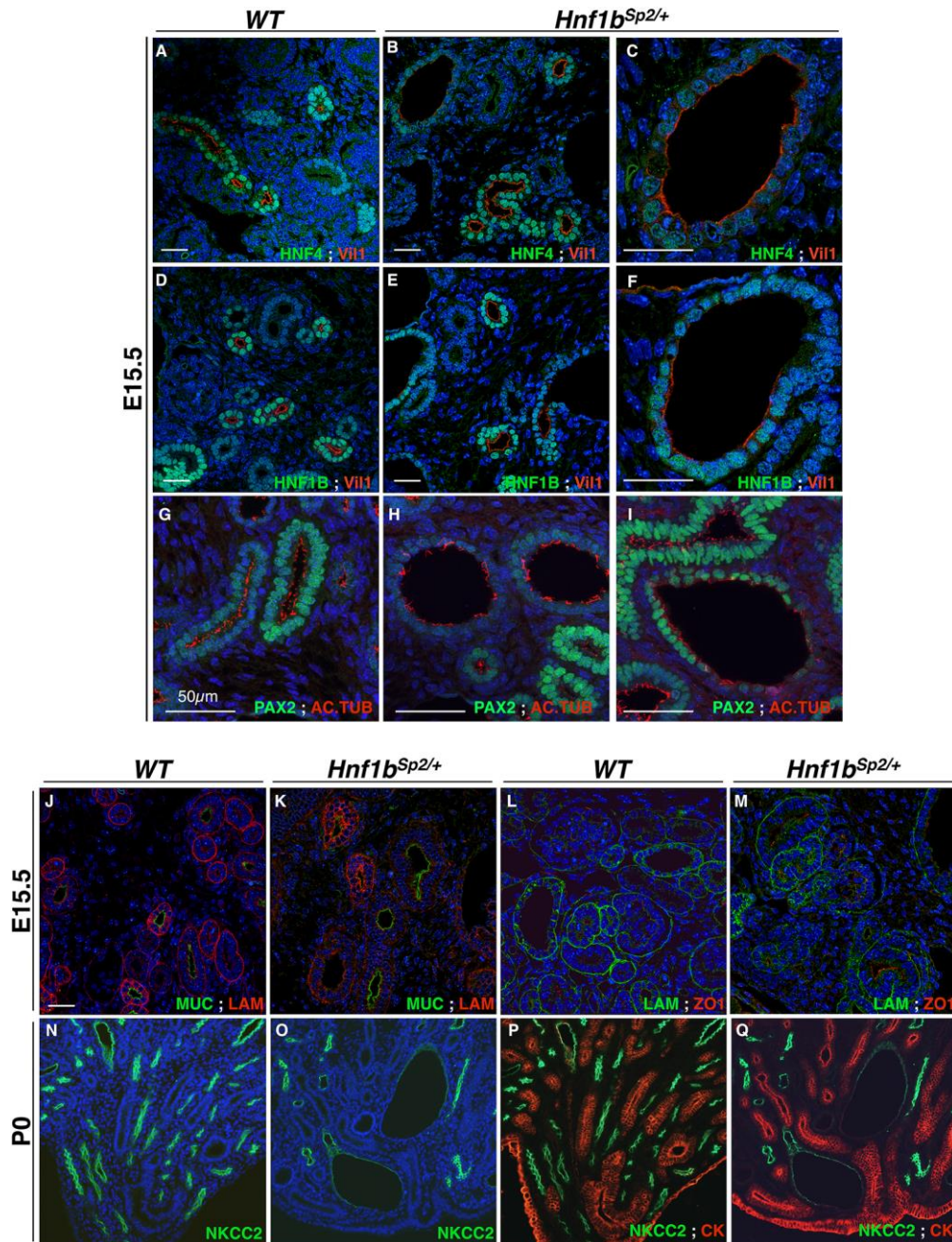


Figure 5: Cystic and dilated PT and thick Loop of Henle cells exhibit abnormal apico-basal polarity and reduced number of cilia.

Confocal microscopy of co-stained sections with Villin (Vil1)-HNF4A and Vil1-HNF1B, revealed that Villin expression (A-F), localized at the PT brush border, is interrupted in several regions of *Hnf1b*^{Sp2/+} cystic structures, indicative of brush-border loss (magnifications in C and F). Confocal images of Acetylated tubulin staining show some regions with cells devoid of primary cilia in E15.5 *Hnf1b*^{Sp2/+} cystic PTs, while non-dilated tubules have apparent normal cilia distribution compared with *WT* (compare H, I with G).

Confocal images of Muc1-Lam1 and Lam1-ZO1 co-immunohistochemistry show that the collecting duct apical marker Muc1 in E15.5 *Hnf1b*^{Sp2/+} (K.) is expressed similar to *WT* (J), while the basement membrane Lam1 exhibit a partial disorganized pattern (K, M) compared to *WT* kidneys (J, L). The tight junction ZO1 is normally expressed. Co-stained P0 kidney sections with NKCC2-CK with NKCC2 (N, O) and merged NKCC2-CK (P,Q) show decreased staining of NKCC2 in *Hnf1b*^{Sp2/+} cystic medullar Loops of Henle (O,Q) as compared with *WT* (N,P). Apical CK expression of collecting ducts (M, N) is not affected. Confocal images were captured with x20 objective (A-N). Optical pictures were captured with x10 objective (O, P) or x20 (P').

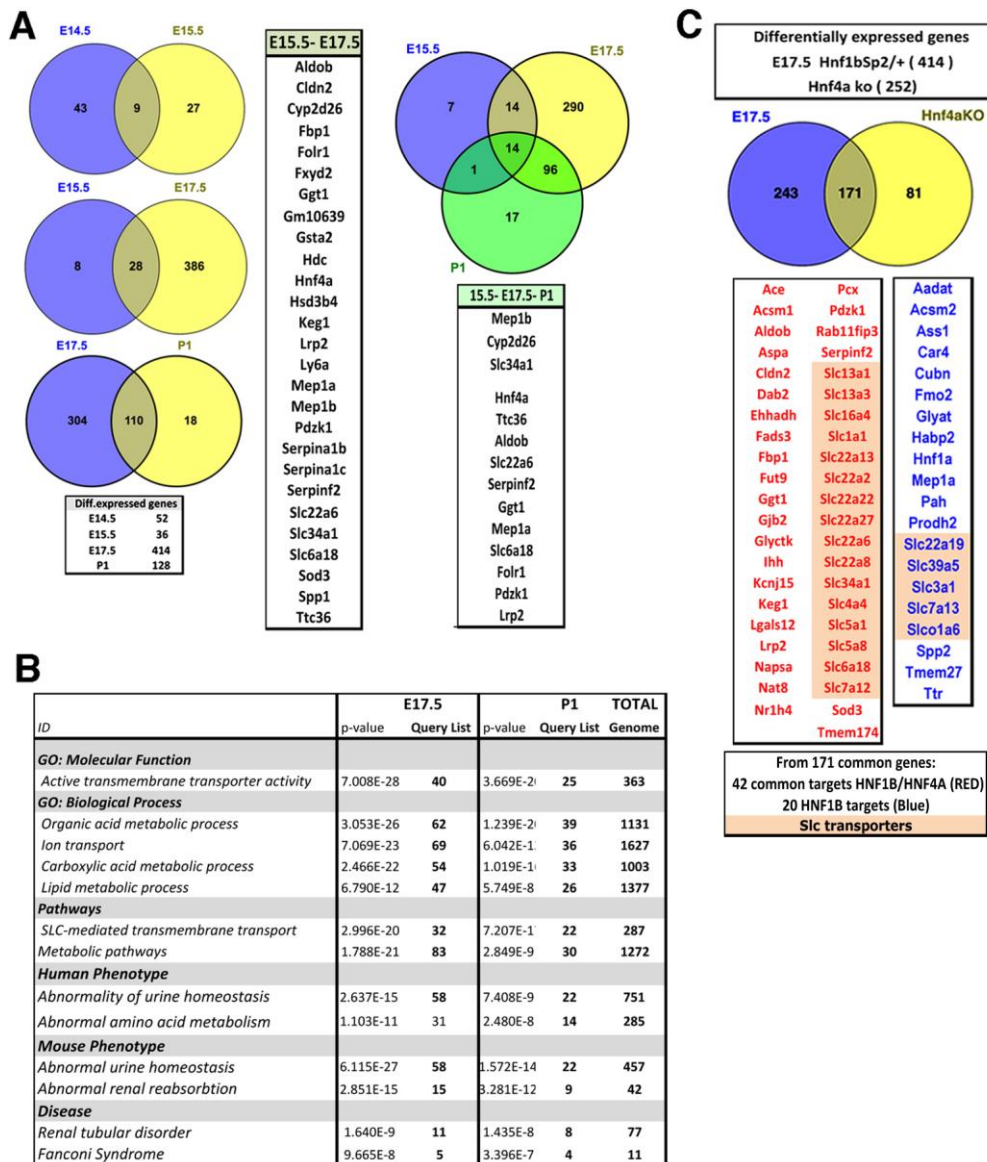


Figure 6: Differential expression analysis in *Hnf1b*^{Sp2/+} mutant versus *s* kidneys at different embryonic stages.

A) Venn diagram showing the overlap of genes differentially expressed from E14.5 to P0. **B)** GO analysis of downregulated genes showing the top enriched terms (Table S5). **C)** Venn diagrams show the overlap of differentially expressed genes of E17.5 *Hnf1b*^{Sp2/+} and P0 *Hnf4a*KO kidneys (Marable et al., 2020). Also indicated are HNF1&HNF4 common target genes (red) and HNF1 targets (blue).

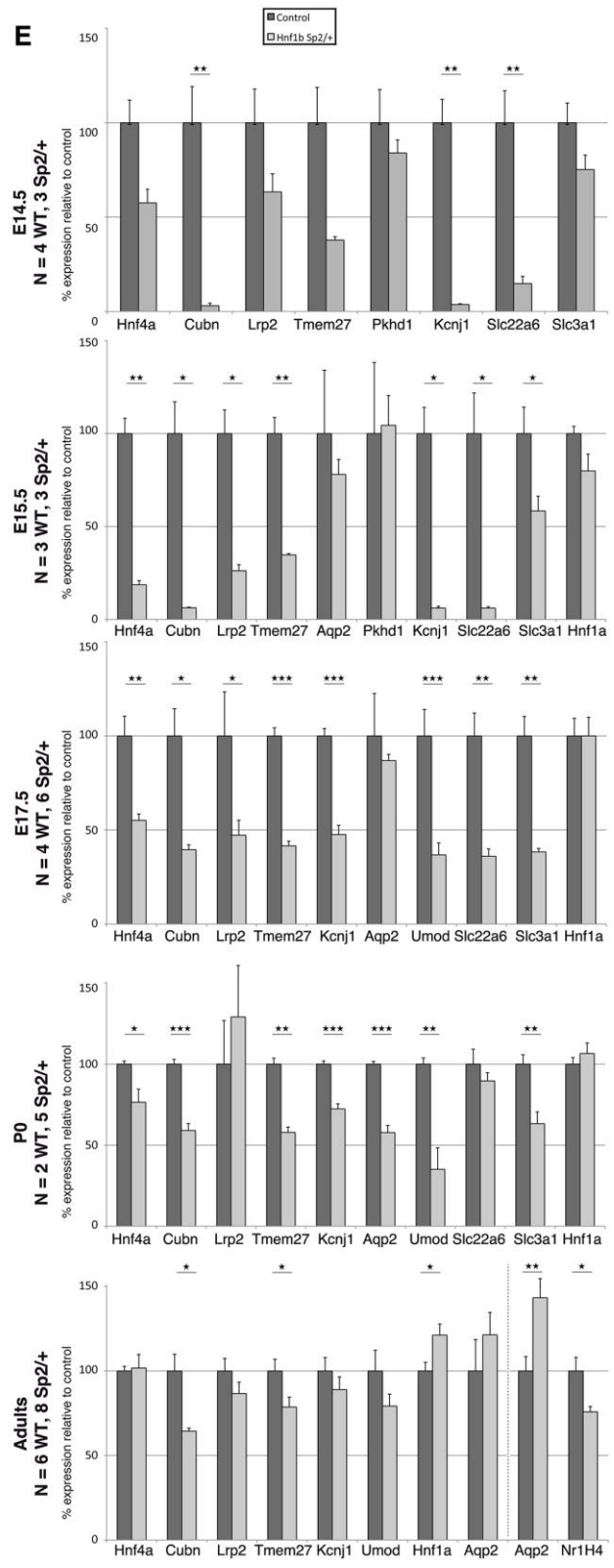
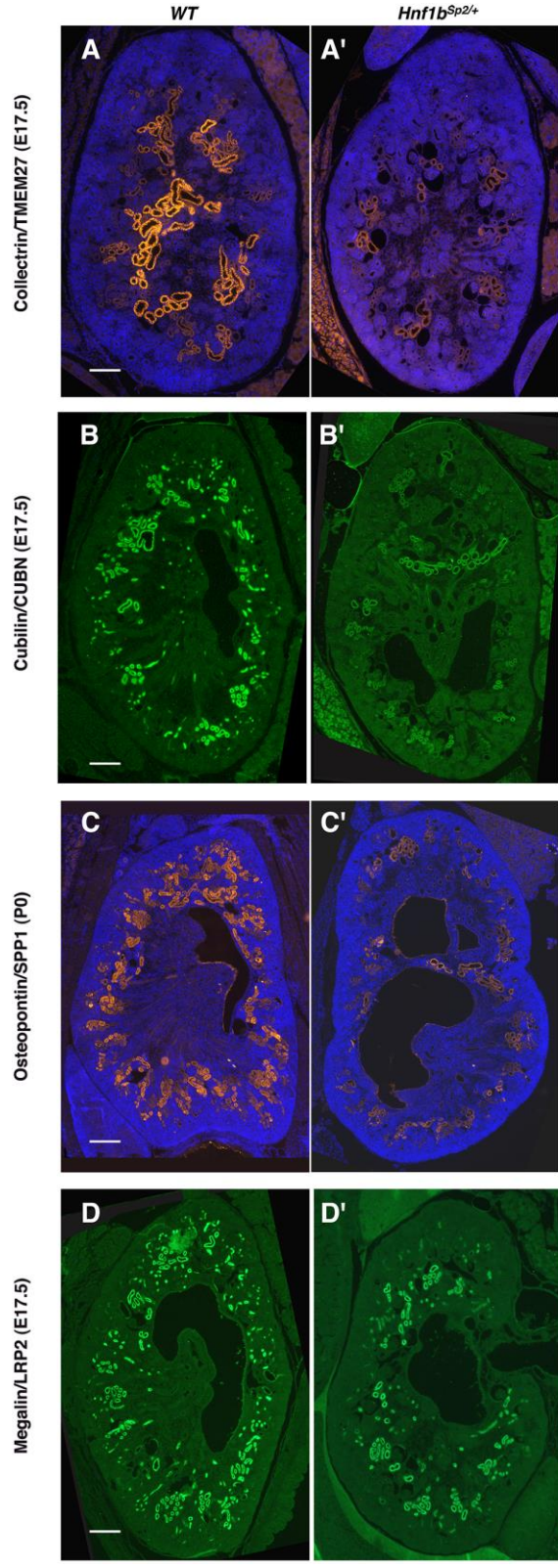


Figure 7: Reduced expression of a subset of HNF1B targets in *Hnf1b*^{Sp2/+} kidneys.

A-D': Representative immunostainings of E17.5 *WT* (A, B, C, D) and *Hnf1b*^{Sp2/+} kidneys (A', B', C', D') show strongly reduced expression in *Hnf1b*^{Sp2/+} kidneys of TMEM27, CUBN and SPP1 (A', B', C'), while LRP2 expression (D') is moderately reduced. E: q-RT-PCR analysis of selected HNF1B targets at different stages show, consistent with mRNA-seq data, significant and strong downregulation of *Hnf4a*, *Cubn*, *Lrp2*, *Tmem27*, *Kcnj1*, *Umod*, *Slc22a6*, *Slc3a1*, during embryo stages up to P0. Also shown q-RT-PCR of adult mice: vertical line separates 3-months from two 6-months samples. *Cubn* and *Tmem27* remained downregulated in adults, while *Aqp2*, downregulated at P0, becomes significantly upregulated in adults (6months). Note downregulation of the target gene *Nr1h4* in adults (6-months). Unpaired t-test, p<0,05 (*), p<0,01 (**) and p<0,001 (***).

Table 1: Urine and plasma parameters of WT and *Hnf1b*^{Sp2/+} mice

Age	3 months		6 months		10-11 months	
<i>Basal parameters</i>	<i>WT</i>	<i>Hnf1b</i> ^{Sp2/+}	<i>WT</i>	<i>Hnf1b</i> ^{Sp2/+}	<i>WT</i>	<i>Hnf1b</i> ^{Sp2/+}
Body weight (BW) (g)	26,1 ± 1,5	<u>23,4 ± 2,4*</u>	<u>29,5 ± 2,8</u>	<u>26,5 ± 3,13*</u>	36,5 ± 2,7	34,9 ± 3,12
Water intake (ml/day)	4,75 ± 0,67	5,01 ± 0,64	<u>3,90 ± 1,43</u>	<u>5,36 ± 1,81*</u>	2,51 ± 1,1	3,4 ± 1,71
Water intake day (20g BW)	3,63 ± 0,51	4,28 ± 0,54	<u>2,64 ± 0,96</u>	<u>4,04 ± 1,36*</u>	1,37 ± 0,6	1,95 ± 0,98
Urine volume (ml/day)	1,24 ± 0,41	1,23 ± 0,73	<u>0,79 ± 0,50</u>	<u>1,61 ± 1,18*</u>	0,72 ± 0,33	0,98 ± 0,38
Urine volume day (20g BW)	0,951 ± 0,31	1,05 ± 0,63	<u>0,535 ± 0,33</u>	<u>1,21 ± 0,89*</u>	0,394 ± 0,18	0,561 ± 0,217
Aliments (g/day)	4,24 ± 0,16	4,23 ± 0,31	3,91 ± 1,46	3,39 ± 0,58	1,22 ± 0,96	1,44 ± 0,9
<i>Urine parameters</i>						
U-Creat (mM)	4,48 ± 0,91	4,11 ± 0,40	5,94 ± 0,88	4,76 ± 1,53	4,29 ± 2,85	3,75 ± 1,84
U-Prot (g/L)	5 ± 2,67	4,7 ± 3,06	7,09 ± 0,85	4,5 ± 2,07	5,07 ± 1,91	5,71 ± 3,67
Mg ²⁺ (mM)	31,9 ± 7	29,4 ± 2,8	<u>35,9 ± 7,2</u>	<u>24,2 ± 2,3*</u>	18,6 ± 10,5	14,3 ± 4,64
Total Mg ²⁺ excreted day	30,33 ± 2,17	30,8 ± 1,76	<u>19,2 ± 2,43</u>	<u>29,2 ± 2*</u>	7,33 ± 3,45	8,03 ± 1
U-Urea (mM)	1376,8 ± 169	1440 ± 135	1264,5 ± 291	1269,3 ± 173	822,7 ± 530	837,7 ± 136
Total Urea excreted day	1309 ± 52	1512 ± 85,2	676,5 ± 98,5	324,14 ± 153	324,14 ± 95,4	469,94 ± 29,6
Na ⁺ (mM)	189 ± 26,1	152,2 ± 10,8*	188,4 ± 29,1	<u>132,3 ± 35,4*</u>	85,2 ± 48,13	98,5 ± 26,2
Total Na ⁺ excreted day	179,73 ± 8	159,8 ± 6,8*	100,79 ± 9,83	<u>160,08 ± 31*</u>	33,56 ± 8,66	55,25 ± 5,6
K ⁺ (mM)	311,3 ± 62,7	272,4 ± 38,6	<u>329,4 ± 41,5</u>	<u>231,8 ± 47*</u>	183,2 ± 88,3	170,2 ± 32,7
Total K ⁺ excreted day	296 ± 19,43	286 ± 24	<u>176,23 ± 14</u>	<u>280,47 ± 41*</u>	72,18 ± 15,9	95,48 ± 7,1
Ca ²⁺ (mM)	1,26 ± 0,41	1,43 ± 0,42	<u>0,94 ± 0,25</u>	<u>1,46 ± 0,18*</u>	1,71 ± 0,57	1,6 ± 0,45
Total Ca ²⁺ excreted day	1,198 ± 0,12	1,57 ± 0,26	<u>0,502 ± 0,08</u>	<u>1,766 ± 0,16*</u>	0,673 ± 0,1	0,897 ± 0,09
U-Pi (mM)	45,4 ± 12	47,9 ± 13,2	70,3 ± 14,2	52,5 ± 17,6	74,8 ± 43	52,5 ± 27,6
Total U-PI excreted day	43,17 ± 3,7	50,29 ± 8,3	37,6 ± 4,7	63,52 ± 15,6	29,47 ± 7,7	29,45 ± 5,9
Cl ⁻ (mM)	242,8 ± 36,0	221,5 ± 19,5	226,5 ± 42,4	224,3 ± 17,8	109,2 ± 73	150,2 ± 48
Total Cl ⁻ excreted day	158 ± 11	232,5 ± 12,2	121,1 ± 14,2	271,4 ± 15,8	43 ± 13	84,3 ± 10,4
Osmolality (mOsm/kg H ₂ O)	2377 ± 445	2196,2 ± 76,3	<u>2893,5 ± 166</u>	<u>2209 ± 271*</u>	1738 ± 751	1583 ± 225
	n=4	n=4	n=4	n=4	n=4	n=4

<i>Plasma parameters (7months)</i>	<i>WT</i>	<i>Hnf1b</i>^{Sp2/+}
Creat (μM)	30,3 ± 2,44	33,3 ± 4,67
Mg ²⁺ (mM)	<u>0,77 ± 0,08</u>	<u>0,89 ± 0,09*</u>
Urea (mM)	7,16 ± 0,84	8,2 ± 1,65
Gluc (mM)	10,7 ± 1,78	11,7 ± 2,02
Ala (U/l)	<u>55,7 ± 14,5</u>	<u>136,3 ± 76,3*</u>
Asat (U/l)	155 ± 60,1	334 ± 282,9
	n=9	n=6

Values are the mean ± SEM corresponding to the average of measurements from 2 or 3 days of urine sample collection under basal conditions at the indicated ages. Urine samples at 3 and 6-months were from the same mice. At 12-months as well as the plasma analysis were from separate groups of mice. Unpaired *t*-test (*) *P* < 0,05. Not underlined = not significant (NS).

SUPPLEMENTARY MATERIAL

Figure S1: Structure and generation of the *Hnf1b* intron-2 spliced mutant mice.

A: Genomic organization of the *Hnf1b* locus, illustrating the 9 coding exons and main functional domains (N-terminal Dimerization, POU-specific (POU_S) and POU-homeodomain (POU_H) and C-terminal transactivation domain). Also indicated are the mutation G to T introduced at the intron-2 splice donor site; the Nuclear Localization Signal (NLS) and the location of the alternative exon of 78 base pairs (bp) present in the *Hnf1b* isoform A (variant A) or without (variant B). **B:** Characterization of abnormal spliced *Hnf1b* transcripts generated by the *HNF1b*^{Sp2/+} mutant allele. Representative semiquantitative RT-PCR from P1- kidney RNA of *WT* (lanes a, b) and *HNF1b*^{Sp2/+} (lanes c, d), using primers located in exon 1 and exon 3 (Material and Methods). Amplifications were performed for different cycles ranging 27 to 36 for *Hnf1b* (lanes a, c and lanes b, d correspond respectively to 30 and 33 cycles) and for *Gapdh*, used to normalize for RNA amount for 24 to 30 cycles, (e, f, show 28 cycles). The structure of spliced products is depicted on the right panel. Sequence of PCR products indicated that *WT* express *Hnf1b* variants A and B, while *Hnf1b*^{Sp2/+} mice express four additional abnormal spliced transcripts corresponding to variants A and B lacking either exon 2 or the last 32bp of exon2 because production of the cryptic splicing site within exon 2 (ss). Quantification of transcript levels normalized by *Gapdh*, in P1 *HNF1b*^{Sp2/+} relative to *WT*, were for the normal transcripts *Hnf1b* (variant A+B) 67% and for the spliced isoforms (A Δexon2 + B Δexon2) 15% and for A+B Δ32pb 14%. The cDNA sequence of spliced isoforms and the encoded truncated proteins from the mutated *Hnf1b* allele are shown in Material and Methods **C:** Cryptic splice site (SS) within exon-2 of mouse *Hnf1b* and human *HNF1B* gene and the 5'splice consensus sequence. Italics show part of the sequence of exon2 spliced out.

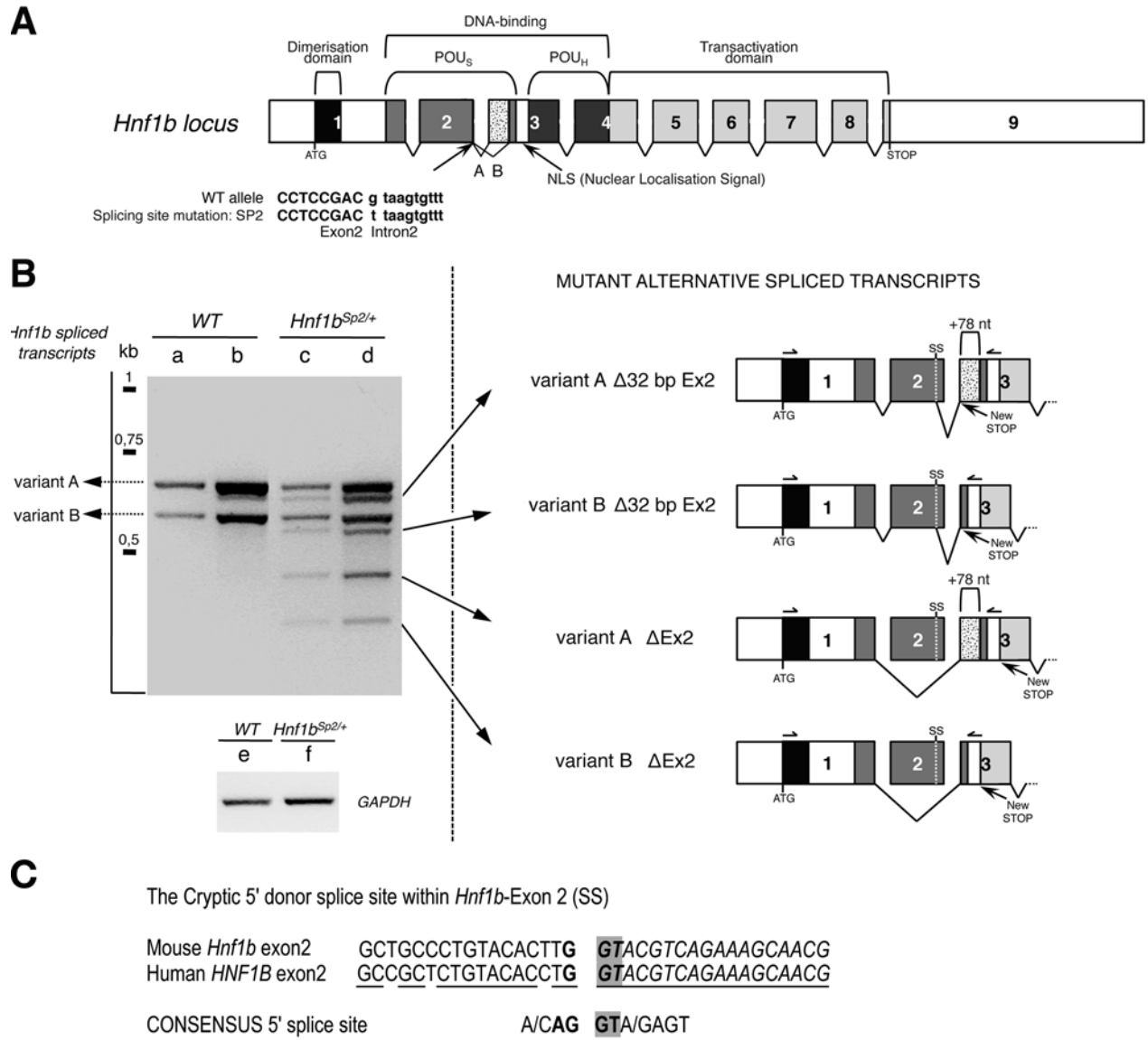


Figure S1

Figure S2: Representative western blots of *WT* and *Hnf1b*^{Sp2/+} kidney extracts at the indicated stages and adult mice. Note that HNF1B isoforms A and B migrate very close and were quantified together. α -tubulin was used to normalize for protein amount as described in Material and Methods. A-C, E: controls corresponding to extracts from transfected cells with expression vectors for HNF1B-variant A (557 amino acids) and for truncated spliced mutant isoforms A Δ exon2 (169 amino acids), B Δ exon2 isoform (143 amino acids) or A/B Δ 32pb (170 amino acids). C: extracts from transfected cells with HNF1B-A, the isoforms A/B Δ 32pb, A Δ exon2 or B Δ exon2 as controls and the indicated increased amounts of E17.5 whole kidney extract from *Hnf1b*^{Sp2/+} showing the absence of truncated isoforms. D shows extracts PO and P1 extracts from respectively the same litters. Dotted vertical line in Panel D (P1), denote that a lane was cut out because of a bubble during transfer, making no possible quantification analysis; otherwise P1 samples were all from the same gel.

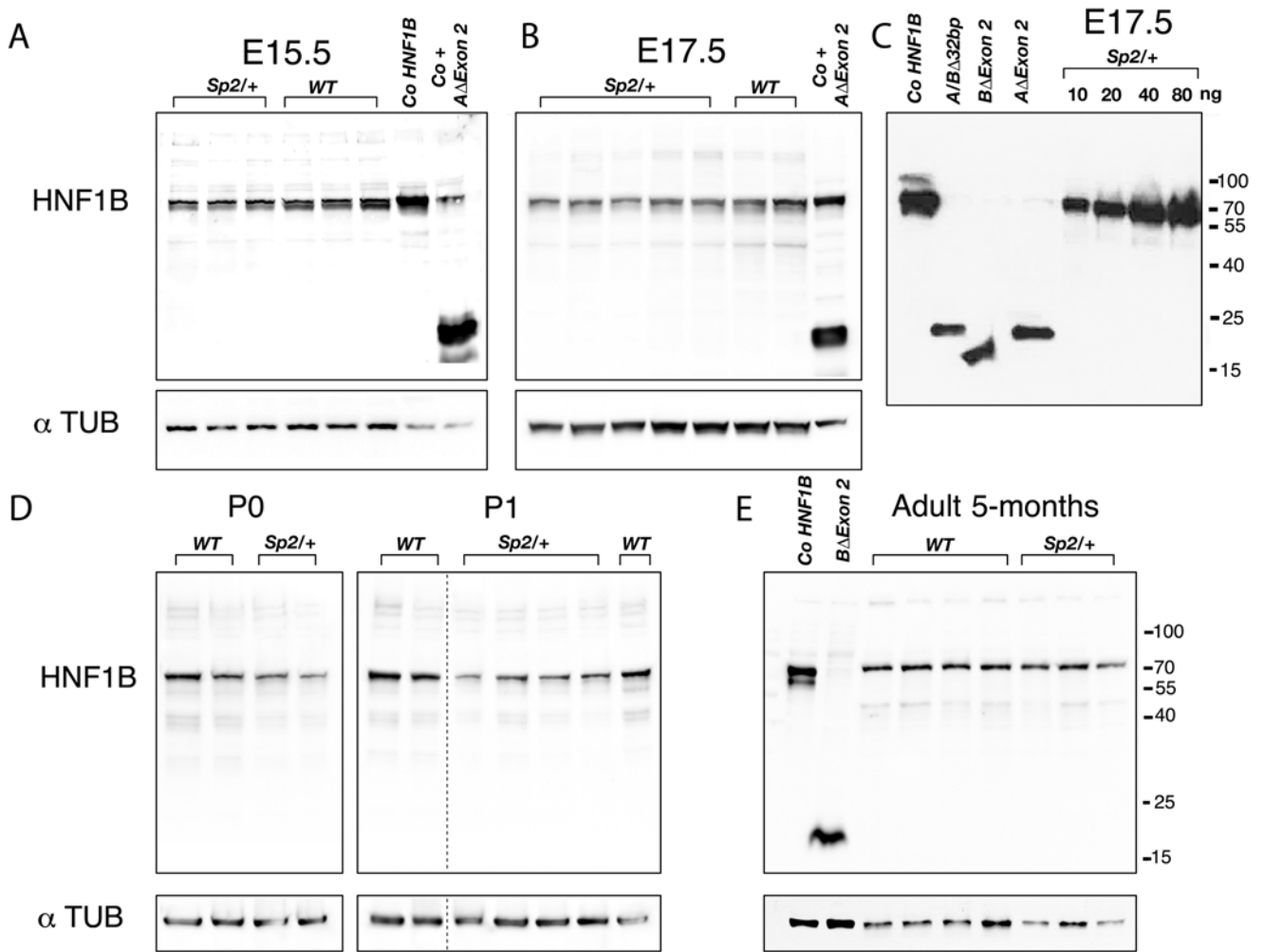


Figure S2

Figure S3: *Hnf1b*^{Sp2/+} E14.5 embryo kidneys show normal histology, branching morphogenesis and nascent nephron structures

A) **Hematoxylin and Eosin (H&E) stained sections:** Upper panel, F1 background (mixed C57BL/6Nx129/sv background), middle panel C57BL/6N and Lower panel 129/sv inbred backgrounds, showing in each case one E14.5 *WT* kidney and the two *Hnf1b*^{Sp2/+} kidneys of the same litter. Scale bar: 200µm.

B) **Immunostainings of Calbindin and PAX-2 show normal expression pattern in E14.5 *Hnf1b*^{Sp2/+} kidneys.** Calbindin-D-28K expressed in the emerging ureteric bud branches, highlights branching morphogenesis, while PAX-2 denotes induced metanephric mesenchyme, UB branches, nascent nephrons, renal vesicles (RV) and S-shaped bodies (SSB) (magnifications in insets)

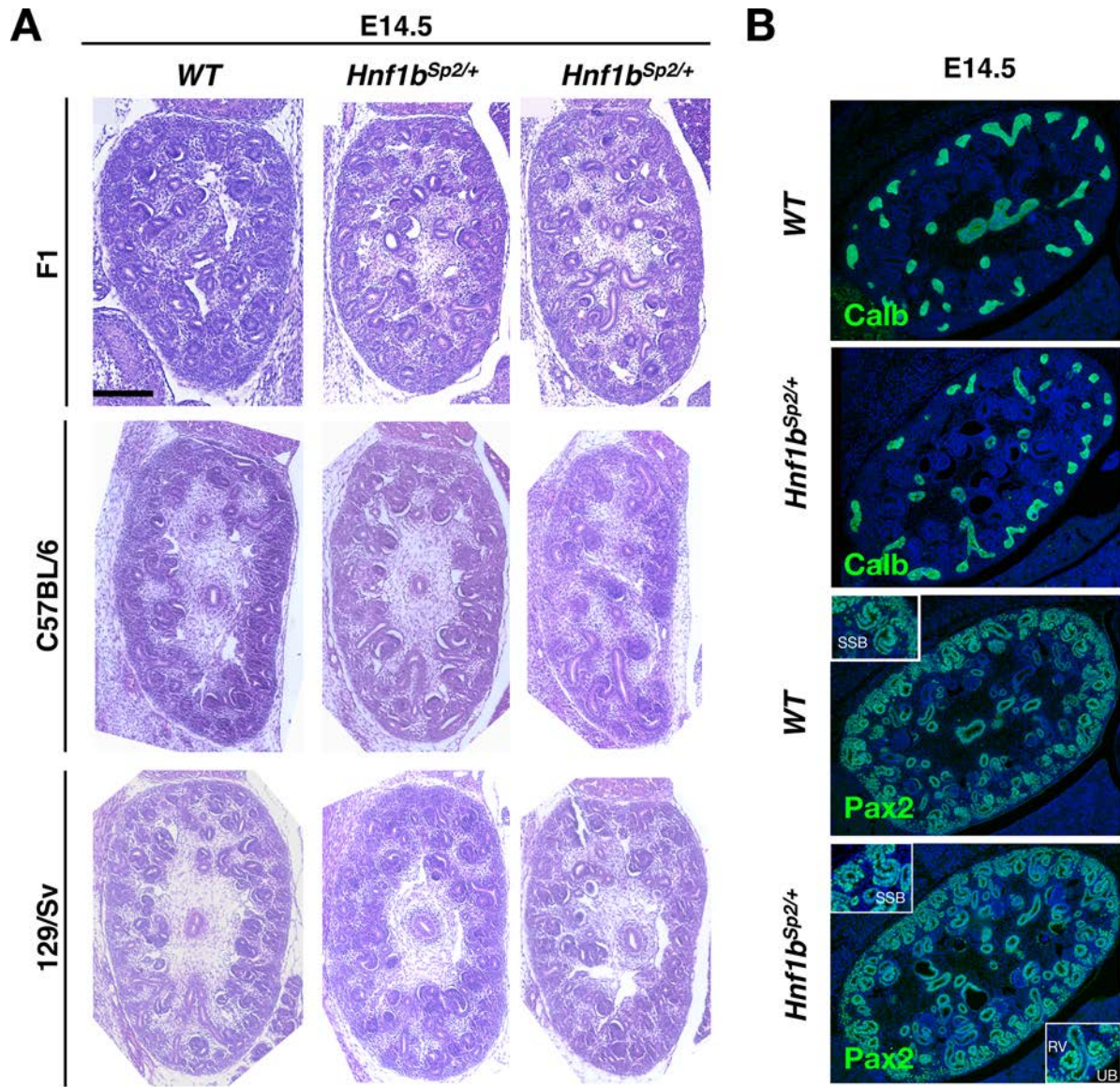


Figure S3

Figure S4: Representative Hematoxylin and Eosin (H&E) stained sections of P0 kidneys in the 129/sv and C57BL/6N background exhibiting increasing severity in the renal phenotype. Note frequent pelvic dilatations and /or hydronephrosis in the C57BL/6N background. The last two C57BL/6N kidney sections correspond to the same *Hnf1b*^{sp2/+} embryo indicating bilateral severely affected kidneys (duplication, hydronephrosis) that would likely be incompatible with life.

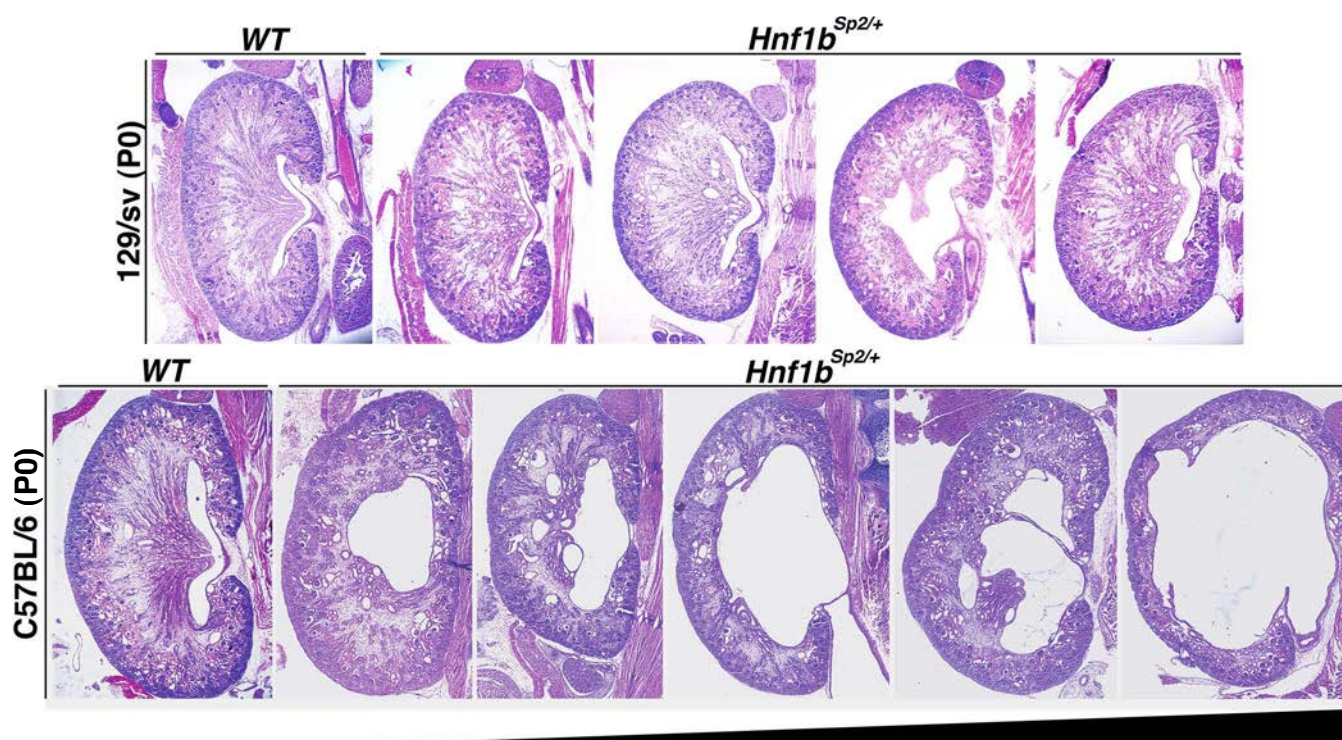


Figure S4

Figure S5: Immunohistochemical analysis of E17.5 and P0 kidney sections show defective proximal tubules cluster size and DBA collecting duct expression.

HNF4A and LTA staining show decreased and unequal clusters of PTs in *Hnf1b*^{Sp2/+} kidneys at E17.5 (A', B') and P0 (F', G'). NKCC2 a marker of the thick ascending Loop of Henle, stains predominantly medullar–cortical cystic structures (C'; H'), AQP2 and CK collecting duct markers express similar to *WT* (D, D'; I, I'; E, E'), while DBA is absent in *Hnf1b*^{Sp2/+} collecting ducts P0 (J'). Sections were co-stained with DAPI. Scale bar: 200µm

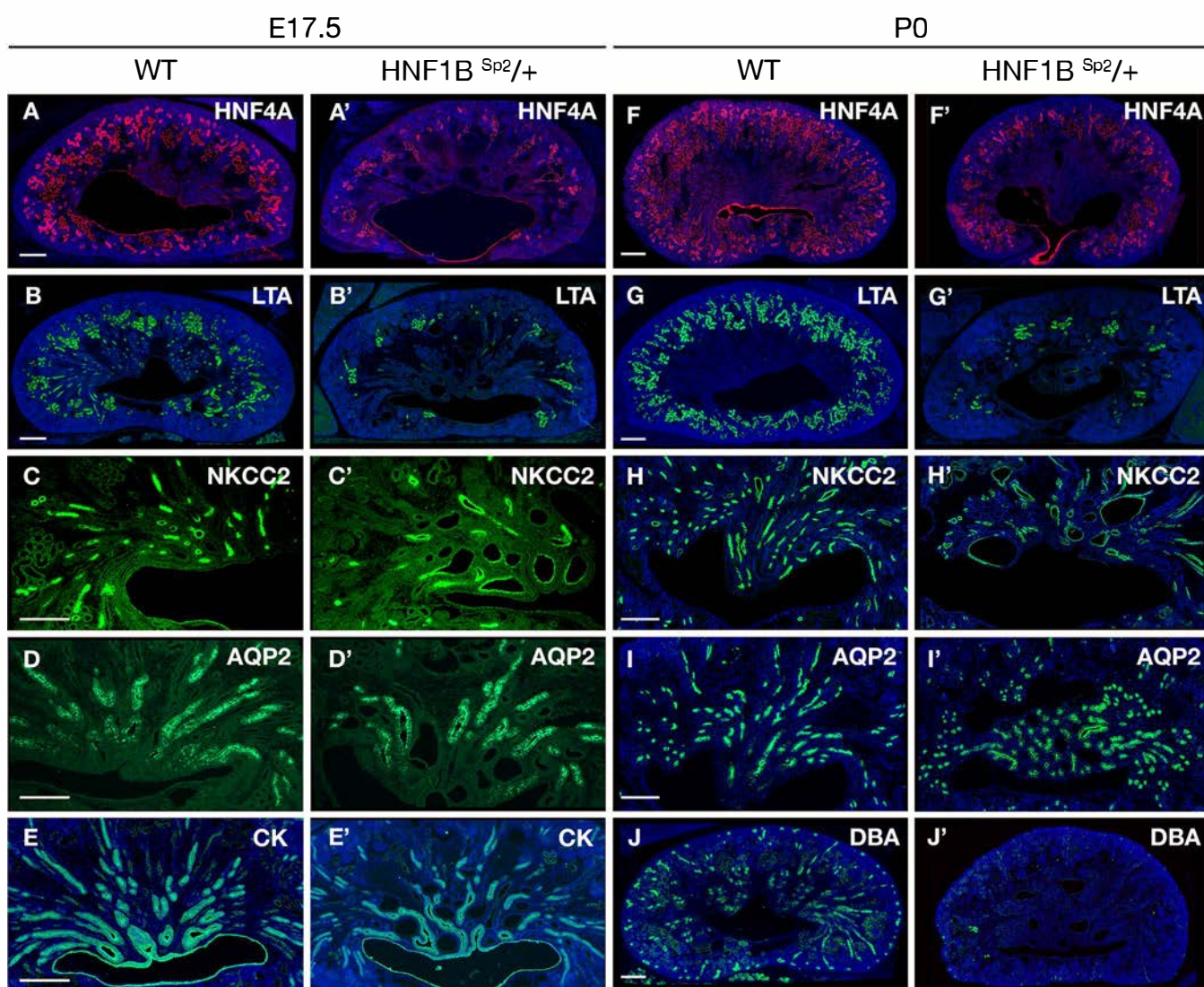


Figure S5

Figure S6: Increased proliferation in *Hnf1b*^{Sp2/+} renal tubules

A) Representative images of phosphohistone H3 (pH3) and HNF4A co-staining of E15.5 embryos show that dilated PTs exhibit an increased numbers of H3P+ cells per structure as compared with *WT*. **B)** Quantification of pH3-positive cells in E16.5 renal tubules of *Hnf1b*^{Sp2/+} (n=8 sections; 3 embryos) indicates an increase of proliferating cells relative to *WT* (n=9 sections; 2 embryos). A higher and significant increase was also observed when compared proliferating cells of *Hnf1b*^{Sp2/+} dilated/cystic tubules versus non-dilated tubules. Note also a significant reduction in the number of renal tubules of *Hnf1b*^{Sp2/+} relative to *WT*, while not significant (NS) changes in the number of nascent nephrons and glomeruli are observed. Unpaired *t*-test. p <0.01 (**) and p<0,0001 (***) are indicated

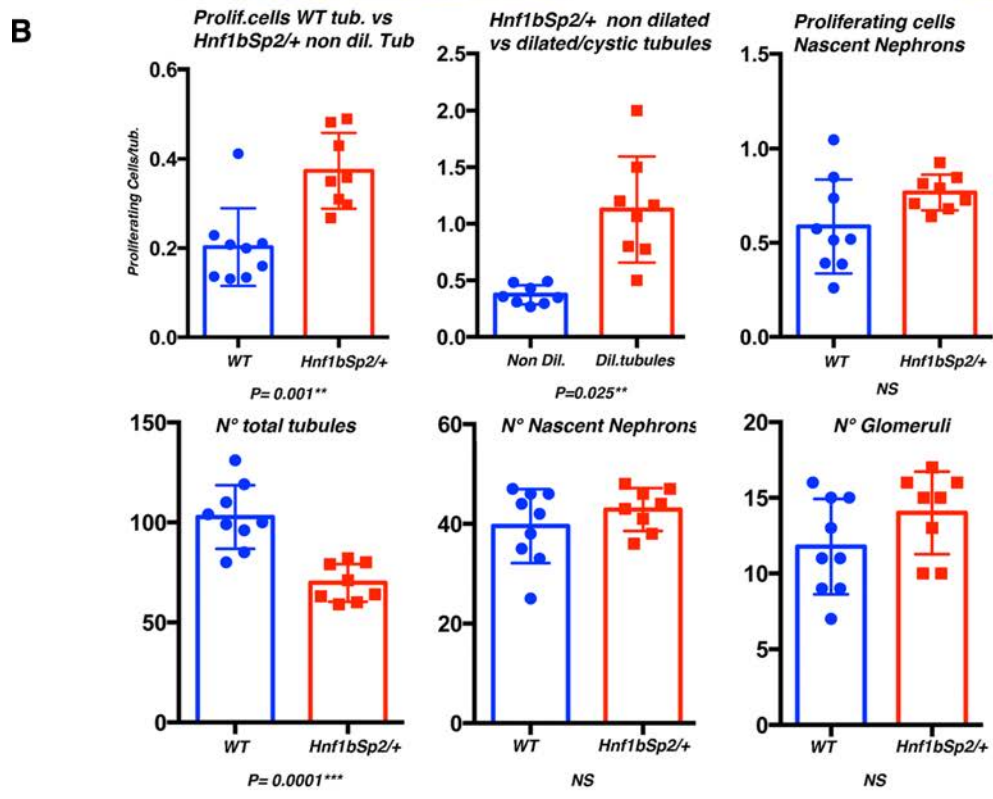
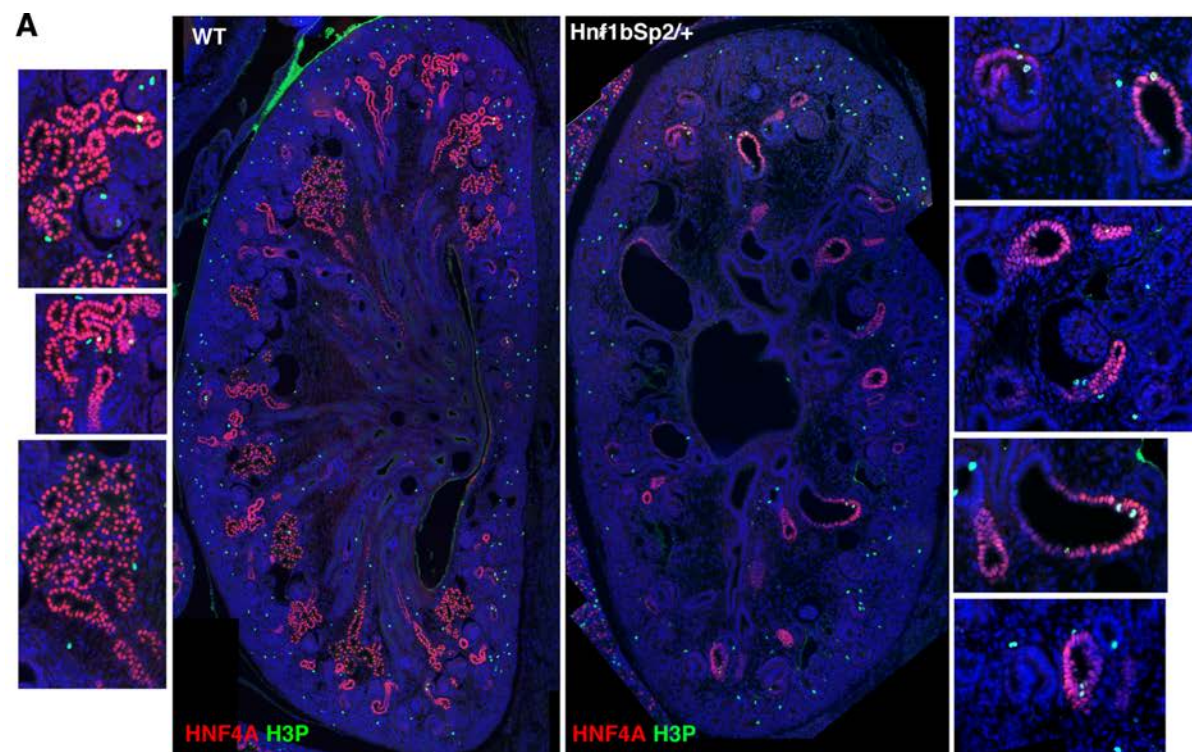


Figure S6

Figure S7: HIS of early proximal tubule anchor genes *Fbp* and *Spp2*. mRNA levels of previously established *Hnf1b* target genes in *WT* and *Hnf1b*^{Sp2/+} at different embryonic stages and at P0.

A: In situ hybridization at E17.5 and P0 of *WT* and *Hnf1b*^{Sp2/+} kidneys show a strong decrease of *Fbp* at both stages and a more modest decrease of *Spp2*. **B:** mRNA levels of the indicated genes at E14.5, E15.5, E17.5 and P0 stages were determined by qRT-PCR and normalized by *cyclophilin-A* expression. Number of *WT* and *Hnf1b*^{Sp2/+} samples used are indicated, n being a pool of the 2 kidneys of each embryo. Values are represented as percentage of *WT* controls. Note the modest and non-significant downregulation of several target genes. Unpaired *t*-test. Significant differences between *WT* and *Hnf1b*^{Sp2/+} ($p < 0.05$ (*)) and $p < 0.01$ (**)) are indicated. Error bars represent standard error of the mean (SEM).

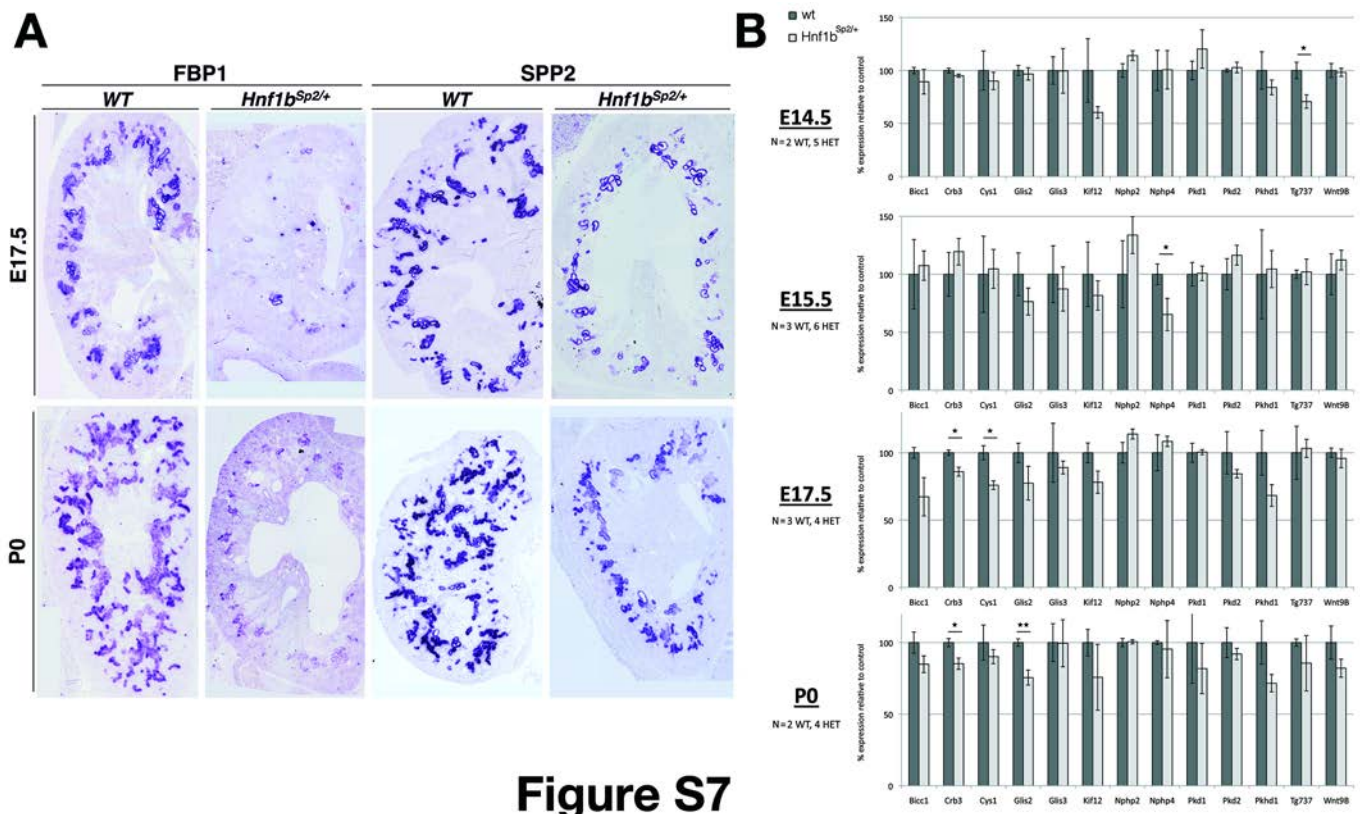


Figure S7

Figure S8: Comparison of different PT markers and previously identified *Hnf1b* target genes in E16.5 *Hnf1b*^{sp2/+} versus *Hnf1a* null kidneys. Note that the PT markers HNF4A, CUBILIN, MEGALIN and LTA are not downregulated in *Hnf1a*^{-/-} embryos (right panel), while are strongly downregulated in *Hnf1b*^{sp2/+} embryos (middle panel) relative to *WT* (left panel) showing that during development the expression of PT genes does not depend on *Hnf1a*.

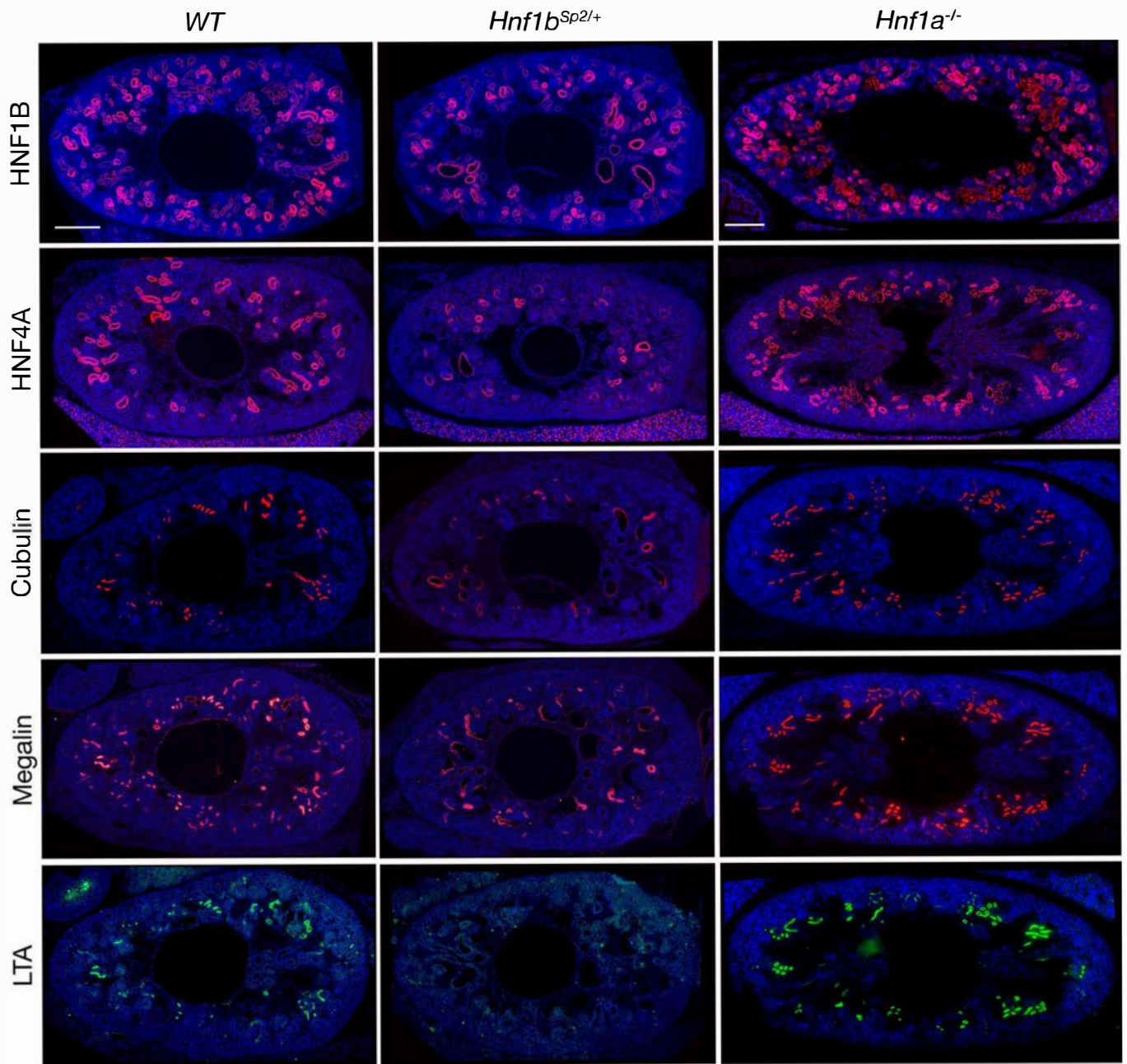


Figure S8

Figure S9: Representative histological sections of adult kidneys from *Hnf1^{Sp2/+}* males and females illustrate disease variation. H&E stained sections of male kidneys of *WT* 12 months (A) and *Hnf1b^{Sp2/+}* (B- F) showing kidney sections of 2month (B), 11 month- (C) 5 month- (D), 17 month- (E), 12 month-old (F). H&E stained sections (G, J, K, L) and trichrome Masson (H, I) stained sections of female kidneys. G: *WT*; H to L of *Hnf1b^{Sp2/+}* of 2-months (H), 12 months (I), 17 months (J), 15 months (K, L). Note clusters of glomerular cysts (magnifications shown in B', E', F', I', I''), microcysts (B, H, I), cell-debris within glomerular cysts (black arrow-heads and surrounding hemorrhagic regions (red arrow-heads), and severe hydronephrosis in both old males (E) and females (L) and rare cases of a severe dysplastic kidney (F). Note no evidence of fibrosis in trichrome Masson stained sections (H, I).

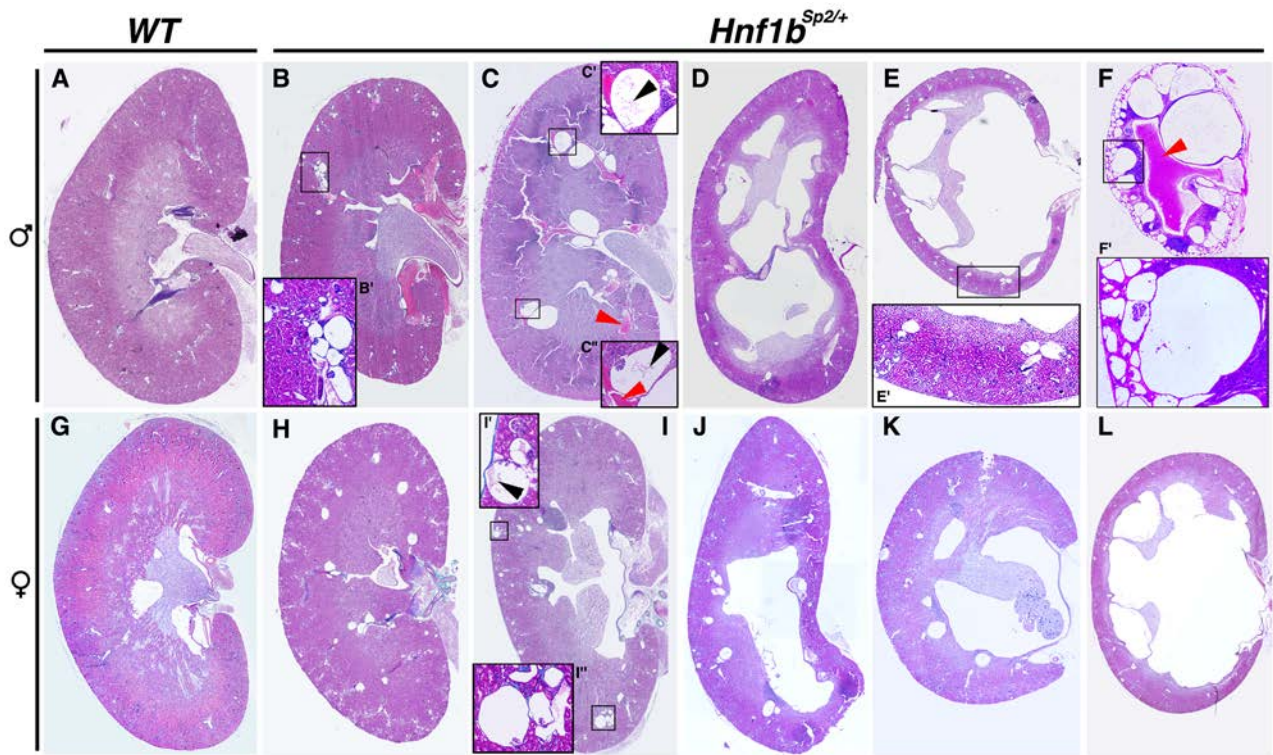


Figure S9

Figure S10: Representative histological sections of the Left and Right kidneys of *Hnf1b*^{Sp2/+} adult males and females, illustrating the variable severity. Body weight curves and kidney weight/body weight ratios. H&E stained sections of the Left and Right kidneys of males (left panel) and females (right panel). **Male Age:** A, A': 17-months; B, B': 13-months; C, C': 10-months; D, D': 16-months; E, E': 9-months; F, F': 17-months; G, G': 17-months; H, H': 12 months. **Female Age:** A, A': 2 months; B, B': 13-months; C, C': 17-months. Unilateral hydronephrosis and pelvic dilatations in 6 to 17 months-old *Hnf1b*^{Sp2/+} mice were observed in respectively 41% and 14 % of *n*=43 males, and 33% and 27% of *n*=18 females. The right lower panel shows body weight curves of males (at the left) and females (at the right) at different ages. Note the tendency of 20% reduction in body weight of both *Hnf1b*^{Sp2/+} males and females, although lower numbers of females were examined. Note also that one month-old heterozygous mutants exhibited lower kidney weight/body weight ratios than *WT* reflecting mild hypoplastic kidneys.

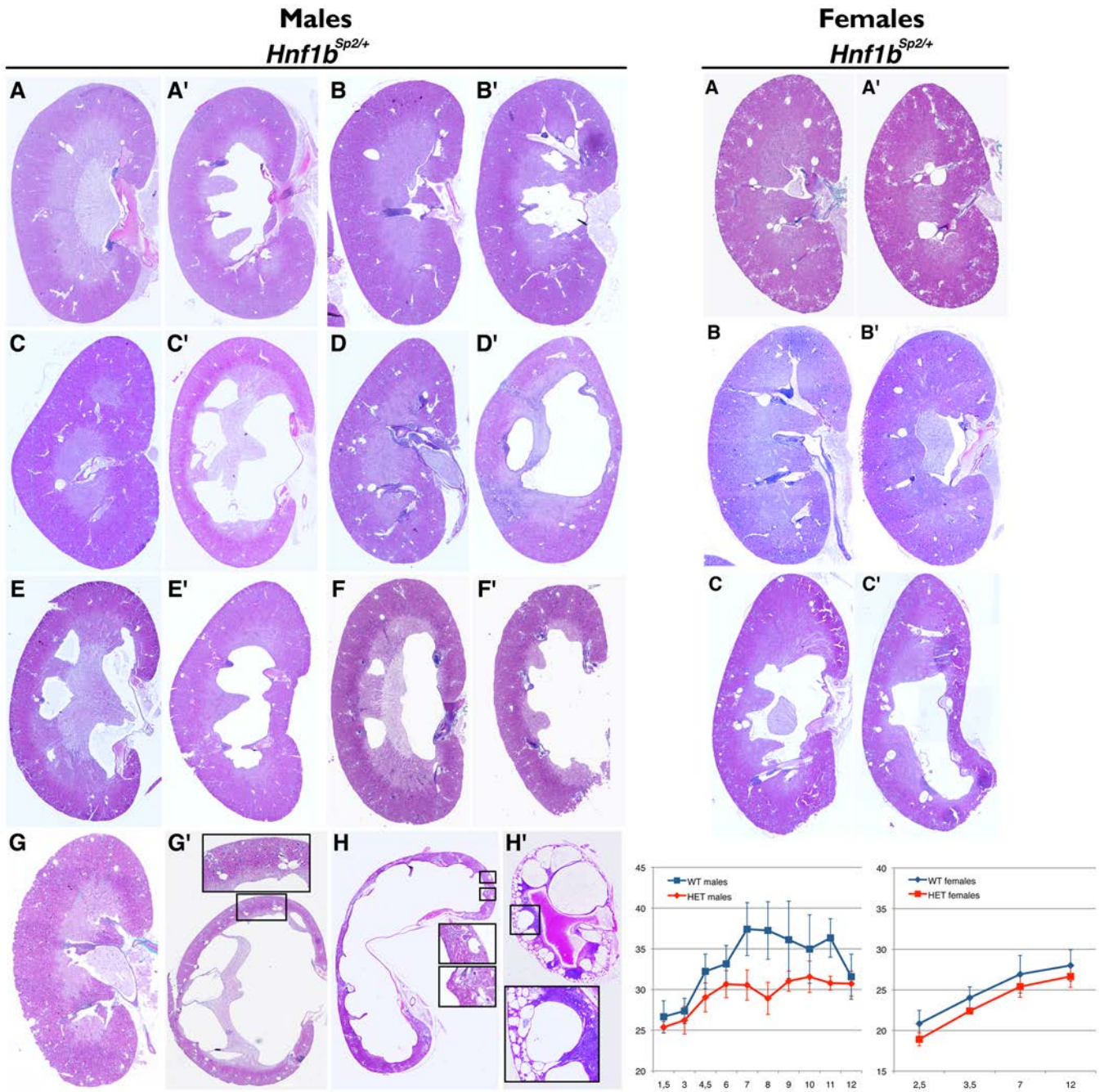


Figure S10

SUPPLEMENTARY TABLES

Table S1: Percentages of renal phenotypes at E18.5 -P0 and Mendelian inheritance**S1A: Percentages of renal phenotypes of *Hnf1b*^{Sp2/+} at E18.5-P0**

<i>Hnf1b</i> ^{Sp2/+} Renal Phenotypes at E18.5-P0	Fi	C57BL/6N	129/sv
N° kidney	28	14	10
Glomerular cysts (%)	82	83	70
Tubular cysts (PT & LOH) %	68	83	80
Pelvic Dilations (%)	3	41*	0
Hydronephrosis (%)		33	0
Duplicated kidney (%)	4	17	0
Bilateral (%)	86	93	80
Severity			
No phenotype (%)	14	0	20
Weak (%)	32	7	50
Moderate to severe (%)	32	43	30
Severe (%)	22	50	0

Phenotypes were defined on the basis of histological analyses of whole kidneys and do not take in account RNA/immunohistochemistry data analyses. WT embryos do not exhibit renal phenotype, but moderate pelvic dilations were observed in 5% of C57BL/N6 WT mice (*), suggesting that the *Hnf1b* splicing mutation exacerbates this phenotype. Note that in case of hydronephrosis, tubular dilations cannot be observed.

Table S1B: Mendelian inheritance in the offspring of *Hnf1b*^{Sp2/+} and WT intercrosses in different mouse backgrounds

Stage	C57BL/6N				129/Sv				F1			
	<i>Hnf1b</i> ^{Sp2/+}	WT	TOT	%HET	<i>Hnf1b</i> ^{Sp2/+}	WT	TOT	%HET	<i>Hnf1b</i> ^{Sp2/+}	WT	TOT	%HET
E14.5	25	32	57	43,8					18	11	29	62
E15.5	13	15	28	46,4	9	9	18	50	9	10	19	47,3
E17.5	13	12	25	52	9	12	21	42,8	16	19	35	45,7
P0	10	12	22	45,4	10	8	18	55,5	20	21	41	48,7
Adult	(125*) (118*)	223	348	35,9	241	265	506	47,6	99	133	232	42,6

Are indicated the number of embryos and/or animals of WT and heterozygous *Hnf1b*^{Sp2/+} mutant obtained from *Hnf1b*^{Sp2/+} males x WT females in the indicated genetic backgrounds, the total embryos or animals (TOT) and percentages of heterozygotes. Numbers with * in C57BL/6N background mice indicate that 7 *Hnf1b*^{Sp2/+} mice died from P1 and P25. The causes of death were not defined due to cannibalism.

Table S2: Primers used for Q- and semi-Q-RT-PCRs			
Gene symbol	Gene name	RefSeq (NCBI)	Primers (5'-3')
<i>Aqp2</i>	aquaporin 2	NM_009699	CCATTGGTTTCTCTGTTACCCTG CGGTGAAATAGATCCCAAGGAG
<i>Bicc1</i>	protein bicaudal C homolog 1 isoform 2	NM_001347189	TGAGGTCAGAACACCTACGA AGTGCAGTGAAGACTGTCCA
<i>Crb3</i>	crumbs family member 3	NM_001347408	CCTGTCTTCAGGGGCTATTG TCGCATGAGCAGAAACAGTC
<i>Cyclo</i>	cyclophilin A	NM_120034.2	CAGGTCCTGGCATCTTGTCC TTGCTGGTCTTGCCATTCT
<i>Cys1</i>	cystin 1	NM_001004455	AGAGGAGCTCATGGCGAGCATT CTGTGGCACAGATGCCAAGAGG
<i>Glis2</i>	GLIS family zinc finger 2	NM_031184	GACGAGCCCCTCGACCTAA AGCTCTCGATGCAAAGCATGA
<i>Glis3</i>	GLIS family zinc finger 3	NM_001305671	TGTGGCATGAATCTCCACCG TGATGGGAGGGATATGTTGACC
<i>Hnf1a</i>	hepatocyte nuclear factor 1 (HNF-1), alpha	NM_009327.3	GTGTAAGTGCACAGGAGGCAAA TTCTCAGTGTCCCAAGACCTA
<i>Hnf1b</i> : WT transcript in <i>Hnf1b</i> ^{Sp2/+} samples	hepatocyte nuclear factor 1 (HNF-1), beta	NM_001291268.1	CGAGGTGGACCGGATGCTCA TCGGAGGATCTCCGTTGCT
<i>Hnf4a</i>	hepatocyte nuclear factor 4 (HNF-4), alpha	NM_001312906.1	CCATCATCTTCTTTGATCCAG CTCACTTGCACCTGTGACC
<i>Ihh</i>	Indian hedgehog	NM_001313683	CCACGTGCATTGCTCTGTCA CACGCTCCCCGTTCTCTAGG
<i>Kcnj1</i>	potassium inwardly-rectifying channel, subfamily J, member 1	NM_001168354	TGTCTCCACGTTTACCCAGCA CGTTGCCGAGAACGCCCAAATA
<i>Kif12</i>	kinesin family member 12	NM_001317352	GAGGCCAATAGCATCAACCG GGAGATGCAGTGGCCCAAT
<i>Lrp2</i>	low density lipoprotein receptor-related protein 2	NM_001081088	AAAATGGAAACGGGGTGACTT GGCTGCATACATTGGGTTTTCA
<i>Nphp2</i>	inversin	NM_010569	ACTTGTACCAGCATATGTGGTC AGGAGAAAACATTTGAACCTTGCTT
<i>Nphp4</i>	nephronophthisis 4 (juvenile) homolog (human)	NM_153424	TTGGCAATAAGCCAGAATCTCC TGATACAGCCTCAACCGTTTGTG
<i>Pkd1</i>	polycystic kidney disease 1 homolog	NM_013630	GCTGCATGCCAGTCTTTTTG TTTTAAAGTGCAGAAAGCCCA
<i>Pkd2</i>	polycystic kidney disease 2	NM_008861	CATGTCTCGATGTGCCAAAGA ATGGAGAACATTATGGTGAAGCC
<i>Pkhd1</i>	polycystic kidney and hepatic disease 1	NM_153179	ATGGAGAACATTATGGTGAAGCC ATGTTTCTGGTCAACAGCCC
<i>Tg737</i>	transgene insert site 737, insertional mutation, polycystic kidney disease	NM_009376	GCAGGCTTCAACCTCATCCTTA TTTCTCCCGATCTCCAATGG
<i>Tmem27</i>	transmembrane protein 27	NM_001313719	TCTATCTGGAATCCGGCAAC CACTCCAGGTGGTCTTTTGT
<i>Wnt9B</i>	wingless-type MMTV integration site family, member 9B	NM_011719	GTGAGAAGGAAGATGGTGAGC GCAGAATCTGGAGAAGCTTGGC
<i>Umod</i>	uromodulin	NM_001278605.1	CTGCACCGATCCTAGTTCCG TCTACCCTGCATTCTTCGCAA

Primers used for semiquantitative RT-PCR

Gene symbol	Gene name	RefSeq (NCBI)	Primers (5'-3')
<i>vATG</i>	hepatocyte nuclear factor 1 (HNF-1), beta	NM_001291268.1	TGGTGTACAGCTCACGTC
<i>V695</i>	hepatocyte nuclear factor 1 (HNF-1), beta	NM_001291268.1	GAGCAGGTGTCTCCGACTGC
<i>Gapdh</i>	glyceraldehyde-3-phosphate dehydrogenase	NM_001289726.1	TCCAGTATGACTCCACTCAC ACCTTGCCACAGCCTTG

Table S3: E14.5, E15.5, E17.5 and P1 transcriptomic profiles (Files 1-4). Shared differentially expressed genes between stages (File 5). Differentially expressed anchor early proximal tubules, proximal tubule, Loop of Henle/distal tubule at E17.5 and P1 (File 6). SLC-transmembrane transporters differentially expressed (File 7). Transcriptomic profile comparisons of *Hnf1b*^{Sp2/+} at E17.5 and P1 and those reported for *Hnf4a* P1 mutant kidney (Marable et al., 2020) (File 8).

[Click here to download Table S3](#)

Table S4: Gene ontology enrichment analysis of downregulated genes at E14.5, E15.5, E17.5 and P1. Selected Gene ontology (GO) terms of differentially expressed genes at different stages (File 5).

GO term enrichment analysis using ToppGene informatics at different stages (Chen et al., 2009), showing the most important GO-terms at each stage.

[Click here to download Table S4](#)

Table S5: Phenotypes of *Hnf1b*^{Sp2/+} adult mice. Kidney-to-body weight ratios and basal parameters of adult *Hnf1b*^{Sp2/+} and WT mice.**A- Percentages of renal phenotypes in adult *Hnf1b*^{Sp2/+} mice**

	<i>Hnf1b</i> ^{Sp2/+}	<i>Hnf1b</i> ^{Sp2/+}
Age: 6-15 months	Males*	Females
Number of mice	48	18
Unilateral hydronephrosis (%)	41	33
Pelvic dilatations (%)	14	27
Glomerular cysts (%)	80	85
Microcysts (%)	25	15
Renal dysplasia/hypoplasia (%)	2	

*Absence of apparent histological phenotype in 8% of males. WTs do not show renal phenotypes, excepted of pelvic dilatations in 3% of C57BL/6N adult mice (males/females).

B: Kidney-to-body weight ratios of WT and *Hnf1b*^{Sp2/+} males

Age	1 month		5 months		10 months		12 months		16-20 months	
	WT	<i>Hnf1b</i> ^{Sp2/+}	WT	<i>Hnf1b</i> ^{Sp2/+}	WT	<i>Hnf1b</i> ^{Sp2/+}	WT	<i>Hnf1b</i> ^{Sp2/+}	WT	<i>Hnf1b</i> ^{Sp2/+}
Body Weight (BW) (g)	20,2 ± 2,6	18,28 ± 0,83	35,1 ± 1,52	29,3 ± 6,46	31,2 ± 2,7	30,1 ± 1,5	37,7 ± 4,38	29,2 ± 1,77	33,1 ± 5,5	30,6 ± 6,2
Left Kidney Weight (KW)	<u>0,14 ± 0,01</u>	<u>0,11 ± 0,02*</u>	0,2 ± 0,02	0,19 ± 0,03	0,22 ± 0,04	0,22 ± 0,04	0,29 ± 0,05	0,17 ± 0,09	0,25 ± 0,06	0,22 ± 0,07
Right Kidney Weight (KW)	<u>0,14 ± 0,01</u>	<u>0,11 ± 0,02*</u>	0,22 ± 0,01	0,23 ± 0,04	0,24 ± 0,04	0,21 ± 0,04	0,26 ± 0,02	0,19 ± 0,001	0,27 ± 0,08	0,22 ± 0,06
KW (left) /BW	<u>0,71 ± 0,05</u>	<u>0,58 ± 0,07*</u>	0,6 ± 0,09	0,66 ± 0,24	0,72 ± 0,07	0,74 ± 0,15	0,77 ± 0,08	0,59 ± 0,13	0,75 ± 0,07	0,72 ± 0,19
KW (right) /BW	<u>0,69 ± 0,05</u>	<u>0,59 ± 0,05*</u>	0,65 ± 0,07	0,79 ± 0,03	0,78 ± 0,11	0,70 ± 0,15	0,72 ± 0,08	0,66 ± 0,05	0,82 ± 0,15	0,72 ± 0,13
Ratio KW (left+right) /BW	<u>1,40 ± 0,1</u>	<u>1,16 ± 0,11*</u>	1,24 ± 0,17	1,45 ± 0,27	1,50 ± 0,15	1,44 ± 0,27	1,49 ± 0,14	1,15 ± 0,18	1,58 ± 0,19	1,44 ± 0,23
	n=3	n=5	n=2	n=2	n=6	n=5	n=3	n=2	n=5	n=11

Values represent the mean ± SEM of the indicated numbers (n) of male mice. Animals with the 2 kidneys to total body weight ratio lower than 1.4 are considered as low. *Hnf1b*^{Sp2/+} kidneys of one-month mice exhibit a moderate hypoplasia manifested by the low kidney-to-body ratio. Note also that there is a bias in these ratios in cases of pelvic dilations of *Hnf1b*^{Sp2/+}. Unpaired 2-tailed *t*-test (*) P <0,05. Not underlined= NS (not significant).

C: Basal parameters of WT and *Hnf1b*^{Sp2/+} males

AGE	5-6 months		12 months	
	WT	<i>Hnf1b</i> ^{Sp2/+}	WT	<i>Hnf1b</i> ^{Sp2/+}
Body weight (BW, g)	31,137 ± 5,622	29,683 ± 3,5	36,5 ± 5,39	35,87 ± 4,9
Water intake (ml/day)	<u>3,909 ± 1,43</u>	<u>5,361 ± 1,81*</u>	2,703 ± 1,196	3,409 ± 0,64
Water intake (20g BW)	<u>2,51 ± 0,91</u>	<u>3,61 ± 1,2*</u>	1,47 ± 0,65	1,9 ± 0,35
Urine volume (ml/day)	<u>0,79 ± 1,43</u>	<u>1,615 ± 1,187*</u>	0,79 ± 1,43	0,79 ± 1,43
Urine volume day (20g BW)	<u>0,507 ± 0,9</u>	<u>1,088 ± 0,79*</u>	9 ± 1,43	1 ± 1,43
Aliments (g/day)	3,91 ± 1,46	3,39 ± 0,58	1,15 ± 0,7	1,58 ± 0,9
	n=11	n=13	n=11	n=14
RATIO	<i>Hnf1b</i> ^{Sp2/+} / WT		<i>Hnf1b</i> ^{Sp2/+} / WT	
<i>Hnf1b</i> ^{Sp2/+} / WT Urine vol 20g BW	2,14*		1,354	
<i>Hnf1b</i> ^{Sp2/+} / WT Water vol 20g BW	1,43*		1,45	

Values are the mean ± SEM and are the average of measurements from 2 days of urine sample collection under basal conditions at the indicated ages. Urine samples were from 3 different groups of mice at 5-6 & 12 months. Unpaired 2-tailed *t*-test (*) P <0,05. Not underlined= NS. n: number of adult males.

TABLE S6 : Differentially excreted urinary peptides between *Hnf1b*^{Sp2/+} and WT mice.

Sequence	Protein name	Accession number	Start (aa position)	Stop	Adjusted p-value	Fold Change
DOWN-REGULATED						
WTDVGMSPRIESASLQGS DRV L	Pro-epidermal growth factor	P01132	620	641	0.0385	-6,27
GRMAHASmGNRPYGP NMANMPPQV GS	AT-rich interactive domain-containing protein 1A	A2BH40	857	882	0.0009	-5,02
PAAPGPAGSPANDNGNGNGNGNG NGGKGKPA	Striatin-interacting proteins 2	Q8C9H6	4	36	0.002	-4,95
LSSLKHPSNIAVDPIERL	Pro-epidermal growth factor	P01132	161	178	0.0028	-4,54
SSLKHPSNIAVDPIERLM	Pro-epidermal growth factor	P01132	162	179	0.0063	-3,7
ALDYDPVESKIYFAQTA	Pro-epidermal growth factor	P01132	522	538	0.0005	-3,7
SGNFIDQTRVLNLGPITR	Uromodulin	Q91X17	590	607	0.0385	-2,81
SSLKHPSNIAVDPIERL	Pro-epidermal growth factor	P01132	162	178	0.0114	-2,78
GAGLEQEEAAG	Heterogeneous nuclear ribonucleoprotein U	Q8VEK3	70	80	0.0494	-2,76
SINKELQNSIIDL	Kidney androgen-regulated prot.	P61110	26	38	0.0385	-2,36
SPRIESASLQGS DRV L	Pro-epidermal growth factor	P01132	626	641	0.0304	-2,18
LVSINKELQNSIIDLLNS	Kidney androgen-regulated prot.	P61110	24	41	0.0448	-2,16
PGApGAPGHPPGPV	Collagen alpha-1(III) chain	P08121	1039	1054	0.002	-1,9
GPpGPpGPpGPpG	Collagen alpha-1(XV) chain	O35206	704	716	0.0436	-1,71
SINKELQNSIID	Kidney androgen-regulated prot	P61110	26	37	0.0132	-1,58
DGQPGAKGEpGDTGVKGD	Collagen alpha-1(I) chain	P11087	809	826	0.0193	-1,54
SpGPDGKTGPpGP	Collagen alpha-1(I) chain	P11087	535	547	0.0117	-1,18
UP-REGULATED						
PGAKGEpGDTGVKGD	Collagen alpha-1(I) chain	P11087	812	826	0.0311	1,29
pGpPGpRGpQGPNADGPQGP	Collagen alpha-1(XI) chain	Q61245	1219	1239	0.0145	1,38
KpGERGLpGEF	Collagen alpha-2(I) chain	Q01149	575	585	0.0466	1,43
GpGERGEHGpGP	Collagen alpha-1(III) chain	P08121	795	807	0.0212	1,53
GlpGTGGpPGENGKpGEpGP	Collagen alpha-1(III) chain	P08121	641	660	0.0032	1,62
NIGFpGPKGSPSGDpGKpGERGHpG	Collagen alpha-2(I) chain	Q01149	497	520	0.0311	1,68
GPpGPTGPAGDKGD	Collagen alpha-1(III) chain	P08121	617	630	0.0348	1,69
GLPpGAPpGEAGKpGEQ	Collagen alpha-1(I) chain	P11087	633	650	0.0009	1,69
GQPpGAKGEpGDTGVKGDAGpGP	Collagen alpha-1(I) chain	P11087	810	832	0.0348	1,74
DGTpGGpGIRGmpG	Collagen alpha-1(III) chain	P08121	526	539	0.0464	1,8
TGPIpPGPAGApGDKGEA	Collagen alpha-1(I) chain	P11087	755	773	0.0287	1,87
GPpGEAGKpGEQ	Collagen alpha-1(I) chain	P11087	639	650	0.0375	1,94
GPIGPpGPAGQpGDKGEGSpGLpG	Collagen alpha-1(III) chain	P08121	764	788	0.0132	2
EAGKpGEQVpGDLGApGP	Collagen alpha-1(I) chain	P11087	643	661	0.0348	2,04
GQpGAKGEpGDTGVKGDAGppGP	Collagen alpha-1(I) chain	P11087	810	832	0.0348	2,16
RDGApGAKGDRGETGP	Collagen alpha-1(I) chain	P11087	1015	1030	0.0032	2,26
GLpGPAGPpGEAGKpGEQGVpG	Collagen alpha-1(I) chain	P11087	633	654	0.0231	2,31
TTGEVKGpGERGLpGEF	Collagen alpha-2(I) chain	Q01149	569	585	0.0375	2,48
GEpGAKGERGApGEKGEG	Collagen alpha-1(III) chain	P08121	818	835	0.002	2,72
AGQpGEKGPpGAQGPpGSpGPLG	Collagen alpha-1(III) chain	P08121	925	947	0.0054	3,06
EVGKpGERGLpGEF	Collagen alpha-2(I) chain	Q01149	572	585	0.002	3,13
pGPAGpPGEAGKpGEQGVpGDLG	Collagen alpha-1(I) chain	P11087	635	657	0.0005	6,9
GpPGEAGKpGEQGVpGDLGApGP	Collagen alpha-1(I) chain	P11087	639	661	0.0008	7,07

Data were obtained from 17 *Hnf1b*^{Sp2/+} and 18 WT mice from 3 to 15 months. 40 peptides with different abundance in urine between the two groups were selected after multiple testing (**Material and Methods**). No differences were observed among different ages. *P* values were defined using Wilcoxon rank-sum test followed by adjustment for multiple testing. Peptides are separated according to *Hnf1b*^{Sp2/+} mice urinary results (up- and down-excreted).

Table S7: List of antibodies

Primary Antibodies	Species	Source	Dilution
HNF1A	rabbit	M. DeVas and J. Ferrer (Imperial College London)	1/100
HNF1B	rabbit	Santa Cruz Biotechnology (H-85 sc22840)	1/100
HNF1B	rabbit	homemade (westerns)	1/500
HNF1B	rabbit	Sigma-Aldrich (HPA002083)	1/500
HNF4a	rabbit	Abcam (ab181604)	1/50
PAX2	rabbit	Covance (PRB-276P)	1/300
AQP1	rabbit	Alpha Diagnostic int. (AQP1 1-A)	1/300
AQP2	rabbit	M. Knepper NIH Bethesda	1/300
NKCC2	rabbit	M. Knepper NIH Bethesda	1/100
Uromuroid (Umod)	goat	MP Biomedicals, Illkrich, France (54140)	1/300
Collectrin	sheep	RD Systems (Ref AF4965)	1/250
LTA-biotin and FITC		Vector lab (FL-1321)	1/200
DBA Biotin and FITC		Vector lab (B-1035)	1/100
WT1	rabbit	Santa Cruz Biotechnology (C19-SC192)	1/200
Laminin	rabbit	Sigma-Aldrich; St. Louis, MO (L9393)	1/100
Calbindin D-28K	rabbit	Chemicon International (AB1778)	1/100
Pan cytokeratin	mouse	Sigma-Aldrich; St. Louis, MO (P2871)	1/50
E-cadherin	mouse	Sigma-Aldrich; St. Louis, MO (610182)	1/200
MUC1	armenian hamster	Neomarkers; Fremont, CA (Muc1 Ab-5)	1/100
Acetylated Alpha - Tubulin	mouse	Sigma-Aldrich; St. Louis, MO (T6793)	1/100
ZO-1	rabbit	Zymed laboratories (40-2300)	1/100
Vil1	rabbit	Sylvie Robine, Institut Curie, France	1/200
CUBN	rabbit	Renata Kozyraki (Cordeliers Research Center)	1/1000
LRP2	sheep	Renata Kozyraki (Cordeliers Research Center)	1/1000
Phospho Histone H3	mouse	Cell Signaling (6G3)	1/200
Alpha-Tubulin	monoclonal	Sigma-Aldrich; St. Louis, MO (T9026)	1/10.000
Secondary Antibodies	species	Source	Dilution
Alexa Fluor 488	rabbit	Invitrogen	1/500
Alexa Fluor 488	mouse	Invitrogen	1/500
FITC Armenian hamster	Armenian hamster	Jackson (127-095-160)	1/500
Biotin rabbit		Vector	1/1000
Biotin mouse		Vector	1/1000
Biotin Goat		Vector	1/1000
Streptavidin-Alexa 594		Jackson ImmunoResearch	1/500
Streptavidin-Alexa 488		Jackson ImmunoResearch	1/500
Peroxidase (westerns)	Rabbit	Jackson ImmunoResearch	1/10.000
Peroxidase (westerns)	Mouse	Jackson ImmunoResearch	1/10.000